UNIVERSITY OF NEVADA - RENO

# Research Report

## Developing a remote sensing protocol and baseline conditions for efficient monitoring of tree crown mortality associated with roads

within the framework of the Marshall Plan Scholarship Program

**Yuanchao Fan**
**9/20/2010**

# Table of Contents

**Preface** ..... 2

**Chapter 1 Assessment of Different Vegetation Indices** ..... 4

1.1 Introduction ..... 4

1.2 Comparison and Assessment ..... 8

**Chapter 2 Assessment of Different Change Detection Methods** ..... 11

2.1 Introduction ..... 11

2.2 Results and Comparison ..... 14

2.2.1 MKT, NDVI Differencing and MSAVI Differencing ..... 14

2.2.2 Post-Classification Change Detection ..... 17

**Chapter 3 Improvement of Ground Reference Data Collection** ..... 22

3.1 Original Ground Reference Data and Its Utility ..... 23

3.1.1 Original Ground Reference Data Collection ..... 23

3.1.2 Calibration Methods ..... 25

3.2 Improved Ground Reference Data Collection Method ..... 35

**Chapter 4 IKONOS Image Preprocessing and Change Detection** ..... 39

4.1 Image Acquisition ..... 39

4.2 Orthorectification and Change Detection ..... 42

**Chapter 5 Other Findings on Remote Sensing Methods** ..... 49

5.1 Improvement on Atmospheric Correction ..... 49

5.1.1 Modification of Atmospheric Normalization Method ..... 49

5.1.2 Absolute Atmospheric Correction using ENVI FLAASH Module ..... 51

5.2 SCS+C Radiometric-Topographic Correction ..... 55

**Conclusion** ..... 57

**Acknowledgement** ..... 58

**References** ..... 58

## *Preface*

The study and research at the University of Natural Resources and Life Sciences, Vienna (Universität für Bodenkultur Wien) within the framework of the Marshall Plan Scholarship program was a very valuable experience. Much was learnt from the people in the Institute of Surveying, Remote Sensing and Land Information, including not only remote sensing methodologies but also enlightenments from this institute's active academic atmosphere. Especially Dr. Werner Schneider and Dr. Tatjana Koukal gave me attentive advising as well as providing me all the necessities for doing the research. Besides, I took graduate level courses on forest ecology, vegetation modeling, applied soil physics and other topics regarding wildlife and the environment.

This report is a summarization of the research work carried out and outcome achieved under the research assignment agreement on the topic: Developing a remote sensing protocol and baseline conditions for efficient monitoring of tree crown mortality associated with roads.

Chapter 1 summarizes the assessment of different vegetation indices that is aimed to find out which vegetation index is the best or most suitable indicator of tree crown health/mortality and if there is a vegetation index that can reduce the influence of external factors and enhance the overall accuracy, in the context of this specific study.

Chapter 2 summarizes the appropriate change detection methods that are applicable to this study, including quantitative approaches based on vegetation index differencing and a new qualitative approach using post-classification change detection. Their power and utility of detecting tree crown mortality or tree health change are assessed.

Chapter 3 includes the important improvement on ground reference data collection method as well as further examination of previously collected ground data. Remarkable enhancement was achieved in the accuracy of calibrating

remote sensing results which will improve the accuracy of statistical analyses later on.

Chapter 4 is the summary of exploring high-resolution IKONOS imagery, which is an important complement to the remote sensing methodology and is completely new in this study since all previous effort was based on coarser-resolution Landsat TM imagery. IKONOS provides an opportunity for fine-scale analyses on road-related tree crown mortality. Image acquisition, preprocessing and initial usage are discussed in this chapter.

Chapter 5 talks about some additional findings regarding satellite imagery radiometric enhancement techniques such as atmospheric correction and radiometric-topographic correction.

As for statistical analyses of road-related effects on tree crown mortality, a thorough analysis is still in progress and has not yet been fully accomplished, due to the schedule of the Lake Tahoe project on which this research assignment is based. The base project aims at statistical methods of utilizing remote sensing results to isolate road-related tree crown mortality. Once this goal is achieved the whole project will be nearly accomplished. Thus this part is out of the scope of this research assignment.

This research has emphasized on developing and improving remote sensing methodology. In-depth investigation and meaningful findings have been made as discussed in the following sections.

# Chapter 1 Assessment of Different Vegetation Indices

## 1.1 Introduction

There are many vegetation indices used to measure and classify the health status of vegetation with remotely sensed data. Vegetation indices are based on the principle that significant differences exist in the reflectance of healthy vegetation, senesced vegetation, and bare soil as a function of wavelength. Information contained in a single spectral band/wavelength is usually hard to interpret and insufficient to characterize vegetation status, thus a lot of vegetation indices have been developed by combining two or more spectral bands in certain forms of mathematical formulas, in order to be capable of indicating relative abundance and activity of green vegetation, which can be described by such parameters as leaf area index (LAI), percentage green cover, green biomass, chlorophyll content, and photosynthetic activity or absorbed photosynthetically active radiation (APAR) (Jensen, 2005). The vegetation index data can be further used in various classification and change detection processes, generating more informative data.

Most vegetation indices can be divided into two general categories: ratios and linear combinations (Jackson and Huete, 1991). The former uses the ratio of any two spectral bands or the ratio of sums, differences or products of any number of bands, such as Normalized Difference Vegetation Index (NDVI); while the latter uses linear combinations of two or more spectral bands, such as Tasseled Cap (Kauth-Thomas) Transformation. They are distinct in that, in spectral feature space, the vegetation isolines (i.e. a constant amount of vegetation with varying soil backgrounds) of ratio indices converge at the origin, while those of linear combination indices remain parallel to the soil line (i.e. the axis of bare soil spectral variation as a function of soil type and/or soil condition).

Many of the vegetation indices make use of the significant difference between red and near-infrared reflectance associated with green vegetation. Reflectance values of near-infrared band generally increase with increasing vegetation cover, whereas those of red band generally behave in the opposite way (Huete and Jackson, 1985). Thus, the combination of red and infrared band from multispectral imagery can be used to

characterize vegetation amount. NDVI is such a vegetation index and is the most often used one for detecting living vegetation canopies. It produces index values ranging from −1 to +1, where higher values indicate more, or healthier, vegetation in a pixel and vice versa. The formula for NDVI is:

$$\mathrm{NDVI} = \frac{\mathrm{NIR}-\mathrm{R}}{\mathrm{NIR}+\mathrm{R}} \tag{1}$$

where, for both Landsat TM and IKONOS imagery, NIR refers to near-infrared band 4 and R refers to red band 3.

Tasseled Cap (K-T) transformation is an example of linear combination indices which produces four orthogonal indices: brightness, greenness, yellowness and nonesuch using four Landsat MSS bands (Kauth and Thomas, 1976). Later, Crist and Cicone (1984) applied the tasseled cap concept to Landsat TM data and produced three orthogonal indices: brightness, greenness and wetness, using all six reflective bands of Landsat TM. The equations are as follows:

$$\begin{aligned} \mathrm{B} &= 0.3037\,TM1 + 0.2793\,TM2 + 0.4743\,TM3 + 0.5585\,TM4 + 0.5082\,TM5 + 0.1863\,TM7 \\ \mathrm{G} &= -0.2848\,TM1 - 0.2435\,TM2 - 0.5436\,TM3 + 0.7243\,TM4 + 0.0840\,TM5 - 0.1800\,TM7 \\ \mathrm{W} &= 0.1509\,TM1 + 0.1973\,TM2 + 0.3279\,TM3 + 0.3406\,TM4 - 0.7112\,TM5 - 0.4572\,TM7 \end{aligned} \tag{2}$$

Here, the brightness feature is defined by the intersection of the plane of vegetation and the plane of soils. Soil variation is two dimensional in the TM Tasseled Cap space and is not equivalent to the primary direction of soil variability. TM brightness is, therefore, not identical to its MSS counterpart that represents a vector pointing along the direction of soil reflectance variation (soil line). However, TM brightness does respond sensitively to change in soil characteristics, because its formula captures variation in total reflectance. It is less responsive to vegetation change. TM greenness is a vector perpendicular to brightness. It is computed to be maximally responsive to the combined effect of high absorption in the visible bands (due to plant pigments and photosynthetic activity) and high reflectance in the near-infrared (due to internal leaf structure and the resultant scattering of near-infrared radiation), which is similar to the contrasting of near-infrared

and red bands in NDVI and is thus able to characterize green vegetation. The wetness feature is defined to correspond to the direction of soil moisture and plant moisture variation and is orthogonal to both brightness and greenness. In the three dimensional space of TM data, brightness and greenness define the plane of vegetation and brightness and wetness define the plane of soil.

The spectral response of vegetation canopy is inevitably influenced by some external factors such as atmospheric attenuation or variations in soil background spectral properties (Colwell, 1974; Huete et al., 1985). Huete et al. (1985) found that the sensitivity of vegetation indices to soil background was greatest in canopies with intermediate levels of vegetation cover, because at intermediate levels, there is enough vegetation to scatter and transmit a significant amount of NIR flux to the soil surface, as well as enough canopy gaps to allow the soil-reflected NIR signal, which strongly resembles vegetation spectral signatures, to reach the sensor. That is why some soil-sensitive indices such as the Simple Ratio index NIR/Red can only be useful at high vegetation densities and Perpendicular Vegetation Index (PVI) can only perform well at low densities, while at intermediate vegetation levels, neither of them can adequately describe the observed behavior of canopy spectra. Atmosphere affects the quality of remote sensing data by scattering and absorption. Shorter wavelengths are more vulnerable to scattering effect and conversely longer wavelengths are mainly subject to atmospheric absorption. For example, the visible bands of Landsat TM (blue, green, red) normally have a higher minimum value due to increased atmospheric scattering taking place in these short wavelengths. Infrared bands, on the other hand, usually have minima close to zero because of atmospheric absorption. Thus, many vegetation indices have been created to minimize atmospheric and soil effects, so as to enhance vegetation sensitivity.

Atmospheric effects can be eliminated in the image preprocessing stage, by either absolute or relative radiometric correction techniques. For deriving vegetation indices from a single image, absolute atmospheric correction was applied to eliminate atmospheric absorption and scattering effects. For change detection, relative radiometric normalization was used. The atmospheric effects in the pair of images used in change

detection were supposed to cancel out each other (see Chapter 5). Therefore, atmospheric effects on vegetation indices will not be discussed later. To test soil background effect and to see if it necessitates a soil-resistant vegetation index in this study, a new index that is most renowned for adjusting soil effects is used in the following and compared with the aforesaid two indices NDVI and K-T transformation that are both sensitive to soil background.

A series of soil-adjusted indices have been created to reduce soil background effect. The first Soil-Adjusted Vegetation Index (SAVI) was proposed by Huete (1988) using a soil-adjustment factor L to account for first-order soil background variations. Baret et al. (1991) developed a transformed SAVI (TSAVI) by taking into account the soil line slope (γ) and intercept (í) (soil line is a linear relationship between bare soil reflectance observed in two different wavelengths), whereas the SAVI assumed them to be 1 and 0, respectively. Qi et al. (1994) presented a Modified Soil Adjusted Vegetation Index (MSAVI) that replaced the general constant L in the SAVI equation with an empirical or inductive L function that was data related and could self-adjust its L value to an optimum. This modification was proved to be of advantage over SAVI and other indices. It produces higher (vegetation) signal to (soil) noise ratio. A study using IKONOS image showed that MSAVI is more able to detect small vegetation patches and overcome soil background effect to a better degree than NDVI. However, it was also noted that MSAVI was more vulnerable to shadow effect than NDVI. It classified shadowed areas more easily as "mixed" containing both vegetation and non-vegetation information (Van Delm and Gulinck, 2009). MSAVI is defined as follows:

$$\mathrm{MSAVI} = \frac{\rho_{\mathrm{NIR}} - \rho_{\mathrm{R}}}{\rho_{\mathrm{NIR}} + \rho_{\mathrm{R}} + \mathrm{L}}(1 + L) \tag{3.1}$$

where L = 1-2γNDVI*WDVI, where γ is the primary soil line slope and WDVI is the weighted difference vegetation index (WDVI = NIR-γR). The inductive version of MSAVI is of this form:

$$\mathrm{MSAVI} = \frac{2\rho_{\mathrm{NIR}} + 1 - \sqrt{(2\rho_{\mathrm{NIR}} + 1)^2 - 8(\rho_{\mathrm{NIR}} - \rho_{\mathrm{R}})}}{2} \tag{3.2}$$

which is based on the same principle as the previous empirical version and has almost the same vegetation sensitivity and soil noise reduction ability. It is also easier to apply to Landsat TM and IKONOS images, so the inductive version will be used.

## 1.2 Comparison and Assessment

Previously, most of the effort was focused on change detection using NDVI Differencing and MKT (see Chapter 2) which are based on NDVI and K-T transformation, but these two vegetation indices themselves had not been used and evaluated independently. Using ground reference data collected at two different points of time to calibrate change detection was hampered by time and sampling method as found in Chapter 2. Single year vegetation indices provide a way to circumvent the problem, because single year ground reference data is much more available and sampling method can be modified any time without worry about previous data. Single year vegetation indices, if chosen properly, can be calibrated by concurrently field-collected ground reference data. The calibrated relationships between current vegetation indices and actual forest canopy attributes (e.g. LAI, healthy canopy cover, and foliage biomass) can be generalized to the same study area for previous years, given that there is little temporal change in soil background and other environment conditions for the same location. Thus previous canopy attributes can be estimated by the vegetation indices using archive images. As long as vegetation change is the main change from time to time, the difference can be reflected in the calibrated vegetation indices of different times and thus change can be detected.

MSAVI, as a new vegetation index, was compared with NDVI and K-T components to see if its soil-adjustment function would take effect and make improvement over the other two. All the three indices were implemented in models by ArcMap model builder using the above Equations 1, 2, and 3.2. Vegetation index images were generated by the models.

Comparison of the performance of these three vegetation indices was done based on their power of predicting real healthy canopy cover or foliage biomass. Field measured tree data were regressed against these vegetation indices generated from synchronous

Landsat TM imagery. Different types of ground reference data including modeled healthy canopy cover or foliage biomass from tree health survey, canopy cover from densiometer, and LAI measured by LI-COR LAI-2000 Plant Canopy Analyzer are analyzed and compared in detail in Chapter 3. LAI data, as shown to be most accurate and have best relationships with vegetation indices, is presented here as the dependent variable. Figure 1a, 1b, 1c and Table 1 show the results of predicting LAI from the above vegetation indices.

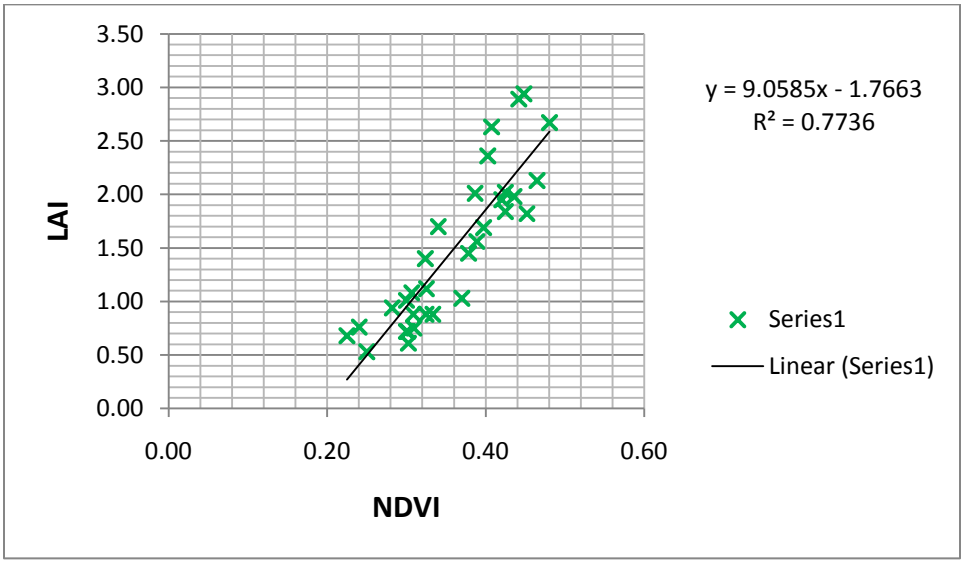


**(a)**

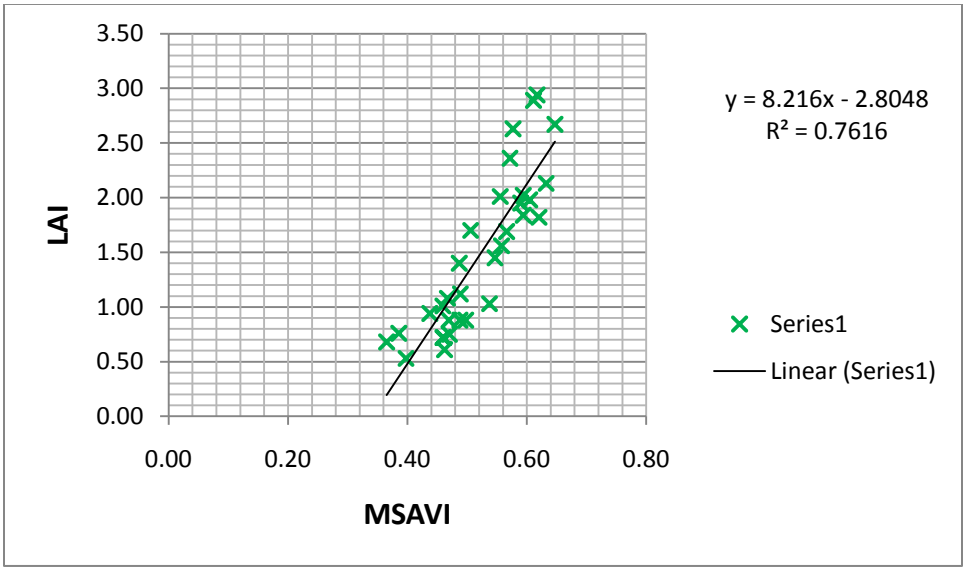


**(b)**

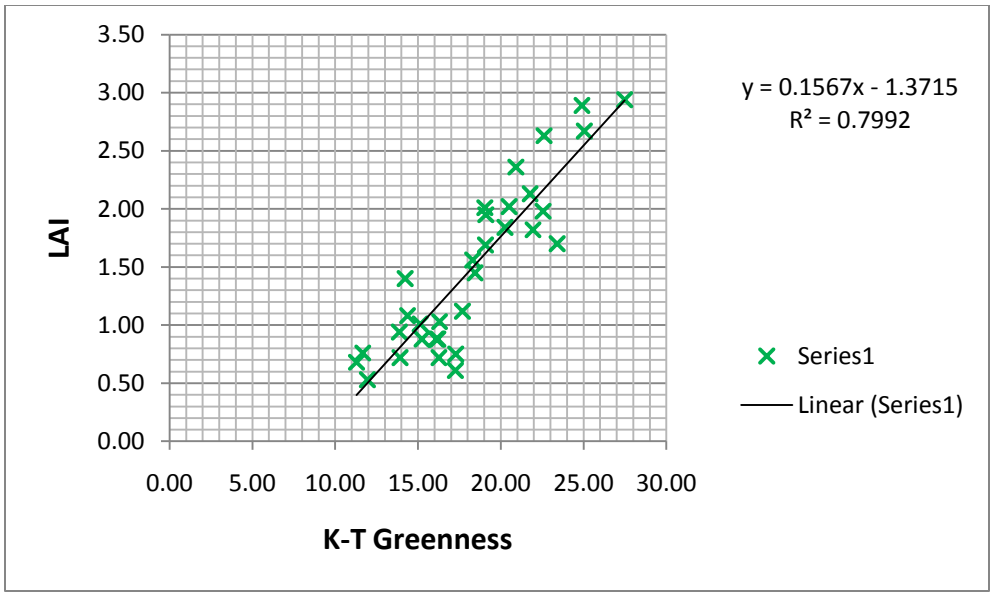


**(c)**

**Figure 1.** Relationship between LAI (measured by LI-COR LAI-2000 Plant Canopy Analyzer) and (a) NDVI, (b) MSAVI, (c) K-T Greenness (derived from synchronous Landsat TM imagery).

| *Regression Statistics* | |
|---|---|
| Multiple R | 0.926481 |
| R Square | 0.858368 |
| Adjusted $R^2$ | 0.843193 |
| Standard Error | 0.284825 |
| Observations | 32 |

ANOVA

| | *df* | *SS* | *MS* | *F* | *Significance F* |
|---|---|---|---|---|---|
| Regression | 3 | 13.766703 | 4.588901 | 56.565342 | 5.276E-12 |
| Residual | 28 | 2.271518 | 0.081126 | | |
| Total | 31 | 16.038221 | | | |

| | *Coefficients* | *Standard Error* | *t Stat* | *P-value* | *Lower 95%* | *Upper 95%* |
|---|---|---|---|---|---|---|
| Intercept | 0.407041 | 0.972146 | 0.418703 | 0.678627 | -1.584310 | 2.398392 |
| K-T Brightness | -0.014299 | 0.014474 | -0.98789 | 0.331667 | -0.043948 | 0.015350 |
| K-T Greenness | 0.141791 | 0.015206 | 9.324622 | 4.402E-10 | 0.110643 | 0.172939 |
| K-T Wetness | 0.001572 | 0.019048 | 0.082546 | 0.934799 | -0.037446 | 0.040591 |

**Table 1.** Multiple Regression results using LAI as dependent variable and Kauth-Thomas (Tasseled Cap) Indices as independent variables.

The above results show that all the indices have significant relationships with field measured LAI. K-T Greenness is the best single predictor, followed by NDVI. MSAVI is slightly worse. When the three K-T components are used together to predict LAI, the R square is the highest (0.858). The P-values in the multiple regression also reveal that among the three K-T components, Greenness is the only significant one; Wetness and Brightness are both not significant. MSAVI which is supposed to correct for soil background effect and enhance the power of predicting real vegetation amount does not show better performance than other soil-sensitive indices in this test. But this does not mean that MSAVI is theoretically a failure in adjusting soil background effect. MSAVI might outperform soil-sensitive vegetation indices in the studies that aim at testing its robustness using models of different soil types. However, in reality, there is not much variation in soil types in a region as small as the Lake Tahoe basin, especially when ground reference data were collected in easy-accessible locations where soils are somehow similar. Moreover, many other random effects such as understory (e.g. grass) noises and LAI measurement errors might cancel each other out. The objective of this study is not to test the advantage of a vegetation index in theory or in model, but to look for the best suitable one for the actual conditions in this specific study area. Kauth-Thomas (Tasseled Cap) indices, therefore, can be said to be the best suitable vegetation indices in the context of this study.

# Chapter 2 Assessment of Different Change Detection Methods

## 2.1 Introduction

Multitemporal Kauth-Thomas transformation (MKT) is formed by a $12 \times 12$ transformation matrix based on the single-date Kauth-Thomas coefficient matrix. Equation 2 in Chapter 1 contains the coefficients defining the first three useful components (Brightness, Greenness, and Wetness) of K-T transformation. Together with other three unnamed components 4, 5, 6, a full set of K-T coefficients form a $6 \times 6$ matrix K. Then MKT is defined by the following $12 \times 12$ matrix M:

$$M=\frac{\sqrt{2}}{2}\begin{bmatrix} K & -K \\ K & K \end{bmatrix} \quad (4)$$

All together 6 stable components and 6 change components are derived when the above coefficient matrix is applied to the 12 bands composed of 6 visible and infrared bands (excluding thermal band) of each Landsat TM imagery from 2 acquisition dates (bitemporal spectral data). Similarly, only the three meaningful change components ΔBrightness, ΔGreenness and ΔWetness are of interest. These three change components are actually the difference of the single-date K-T components normalized by a factor: $\sqrt{2}/2$. MKT calculation model was built by the ArcMap model builder. Below is a snap shot of the model:

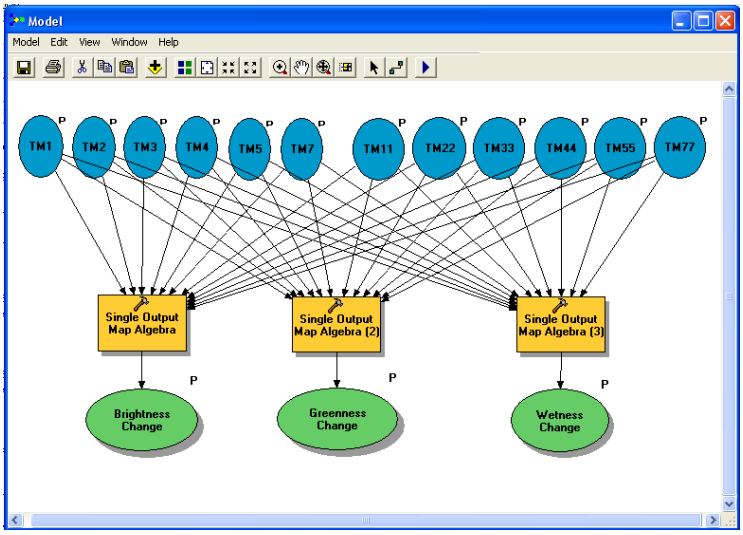


**Figure 2.** A picture of the MKT model built in ArcMap. TM1 to TM7 are the inputs of 6 bands (except thermal band) of Landsat TM imagery from an earlier year and TM11 to TM77 are the counterpart inputs from a later year. Functions are written in the map algebra. Outputs are the three MKT change components.

Collins and Woodcock (1996) applied this method to the same study area as my project. Its performance was highly commended in this paper based on comparison with multi-date Principle Component Analysis (PCA) and Gramm-Schmidt orthogonalization (GS) methods. I will compare the result from my study with this paper. One thing to note is that MKT coefficients for reflectance data are different from those for raw DN data. Thus, when images were pre-processed to scaled reflectance data (e.g. absolute atmospherically corrected), a different set of coefficients were used.

NDVI Differencing and MSAVI Differencing change detection methods simply create a difference image by subtracting the NDVI image and MSAVI image, respectively, of the earlier year from that of the later year.

Different from MKT, NDVI Differencing and MSAVI Differencing which are all based on mathematical manipulation of original images, Post-Classification Change Detection is based on independent classification of each image from multiple dates, followed by a pixel-by-pixel or object-by-object comparison using a "from-to" change detection matrix to detect changes. The former three change detection techniques generate quantitative change values without from-to change class information, while the latter cannot give quantitative change values but it is able to provide detailed "from-to" change class information. The trial of this new change detection method (Post-Classification Change Detection) is aimed to test whether it is able to classify pixels with salt-damaged vegetation and others with healthy vegetation so that the degree of salt damage and direction of change can be detected. If this method works, it will provide a different approach to modeling road-related tree crown mortality.

As for the previous MKT and NDVI Differencing methods, resulting images with quantitative change values were used to model tree crown mortality by calibrating a regression equation with ground reference data. The modeled mortality values, however, contain mortality caused by many different factors including, but not limited to, de-icing salt damage (road-related), disease, insects, and drought (non-road-related). To isolate the component of tree crown mortality that is road-related from that which is apparently caused by other factors, regression analyses have to be applied to examine if a significant relationship between tree crown mortality and road-related variables can be found. We can first predict tree crown mortality as a function of non-road-related variables, and then test for the significance of road effect by a partial regression plot showing the effect of adding road-related variables one by one to the regression model. In Post-Classification Change Detection, such statistical analyses are not necessary if only the spectral signature of de-icing salt damage can be properly found in the multiple bands of remote sensing imagery. Each single year classification image already indentifies pixels with a certain

level of salt-damage, though only in a qualitative manner, because field mortality data is used as classification signature/training data.

## 2.2 Results and Comparison

### 2.2.1 MKT, NDVI Differencing and MSAVI Differencing

Three quantitative change detection methods have been conducted. Their performances are compared by their goodness of fit when calibrated with ground reference data. The test of Post-Classification Change Detection method will be discussed individually.

The three major change detection algorithms: MKT, NDVI Differencing and MSAVI Differencing are based on the three corresponding vegetation indices as introduced before, so the comparison of the relationships between these change detection results and field-measured tree health change is also an indirect comparison of the vegetation indices' ability. However, different from previous chapter, directly calibrating change detection results requires ground reference data collected at two different points of time concurrent with the image collection dates. This means ground reference data collections have to be planned in advance and there has to be a long time interval between the initial collection and repeated collection to allow a significant change in tree health. In this study, different types of ground reference data were collected and data with one to three-year interval were used. The assessment of different types of ground reference data will be discussed in Chapter 3. The healthy canopy cover change data of the 30 plots from 2006 to 2009 derived by DBH-Crown Radius allometric model and rescaled by health status rating (Equations 5 and 7) are chosen to be the dependent variable in the following regressions.

MSAVI difference image was created for the first time in the work reported here. MKT greenness, brightness and wetness images, and NDVI difference image were created previously. They were used as independent variables in the regressions to predict field-measured healthy canopy cover change. For MKT its greenness component was used as a single predictor, in addition to the multiple regression using all three change components.

As seen in Figure 3, all the regressions show significant relationships. Different from previous single-year calibration (Section 1.2 Figure 1), ΔNDVI has the strongest power of predicting healthy canopy cover change as a single predictor. The differences in prediction power between three change detection methods are enlarged compared to that found in Section 1.2. The regression against ΔMSAVI, which was supposed to eliminate soil background effect and enhance the overall accuracy, has the lowest R square (0.4556), 32% lower than that of using ΔNDVI (0.6737). When multiple regression was performed using MKT ΔGreenness, ΔBrightness and ΔWetness, the R square was the highest: 0.72. Different from previous single-year calibration where K-T Greenness was the only significant variable (Table 1), here among the three MKT components, both ΔGreenness and ΔBrightness are significant at 0.5% level. ΔWetness is still not significant at all. This finding strongly contrasts with Collins and Woodcook's (1996) conclusion on the same study area that MKT ΔWetness is the most reliable single indicator of forest change.

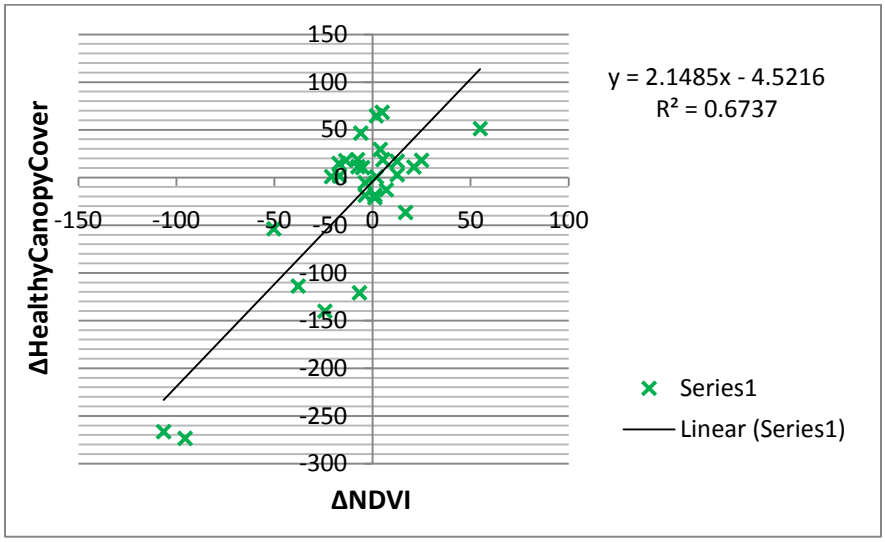


**(a)**

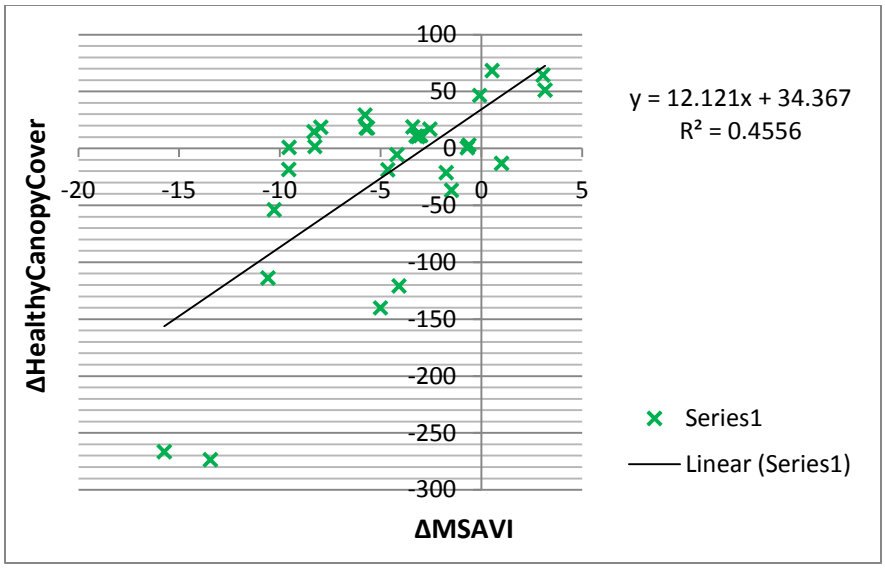


**(b)**

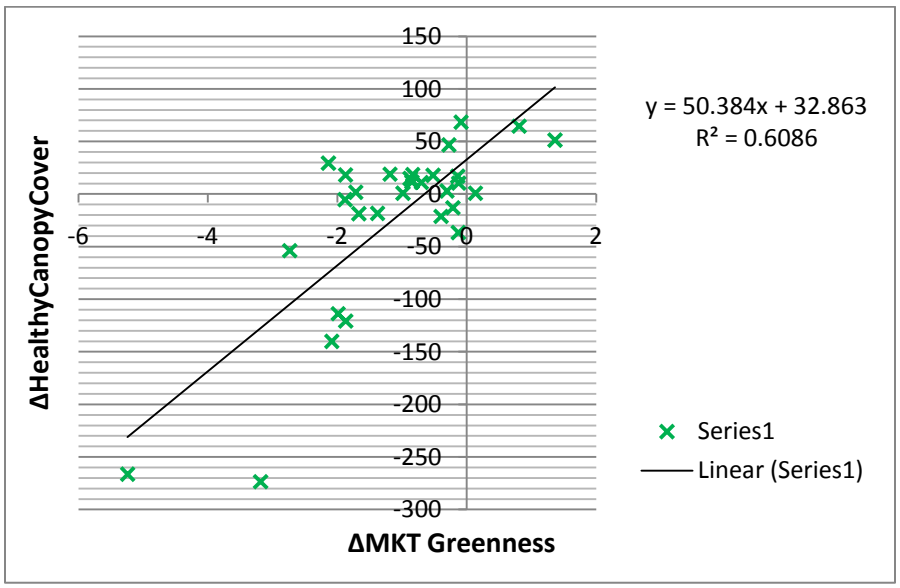


**(c)**

**Figure 3.** Relationship between Δ Healthy Canopy Cover (derived from ground reference data using Equation 7) and (a) ΔNDVI, (b) ΔMSAVI, (c) MKT ΔGreenness (derived from 2006 and 2009 anniversary Landsat TM images). Change detection values were rescaled by 1000.

| *Regression Statistics* | |
|---|---|
| Multiple R | 0.849043 |
| R Square | 0.720874 |
| Adjusted $R^2$ | 0.688667 |
| Standard Error | 46.33475 |
| Observations | 30 |

ANOVA

| | *df* | *SS* | *MS* | *F* | *Significance F* |
|---|---|---|---|---|---|
| Regression | 3 | 144160.4 | 48053.47 | 22.38263 | 2.25E-07 |
| Residual | 26 | 55819.64 | 2146.909 | | |
| Total | 29 | 199980 | | | |

| | *Coefficients* | *Standard Error* | *t Stat* | *P-value* | *Lower 95%* | *Upper 95%* |
|---|---|---|---|---|---|---|
| Intercept | 5.502165 | 14.77009 | 0.372521 | 0.712525 | -24.8582 | 35.86253 |
| MKT-ΔBrightness | -6.014275 | 1.9564 | -3.07415 | 0.004912 | -10.0357 | -1.99284 |
| MKT-ΔGreenness | 36.963278 | 8.417737 | 4.391118 | 0.000168 | 19.66037 | 54.26618 |
| MKT-ΔWetness | -3.048918 | 2.088817 | -1.45964 | 0.156367 | -7.34254 | 1.244705 |

**Table 2.** Multiple Regression results using Δ Healthy Canopy Cover as dependent variable and MKT ΔGreenness, ΔBrightness and ΔWetness as independent variables.

### 2.2.2 Post-Classification Change Detection

IKONOS images were used for classification instead of Landsat TM for two reasons: (1) IKONOS has higher spatial resolution (4m), which enables analyses of road-related effects on tree health. The 30-m resolution of Landsat TM is too coarse for a fine-scale analysis, because the overall mean zone and maximum range of influence from de-icing salt was found to be around 30.2 feet (10m) and 102 feet (30m), respectively, from the edge of highway pavement in previous field-based studies. (2) IKONOS has much higher radiometric resolution by virtue of its 11-bit data depth. Compared to the 8-bit data of Landsat TM, 11-bit data capture much more subtle differences of radiometric intensity in the pixels or reflectance of the objects. It is thus especially suitable for classification of different levels of tree health status.

Sep-25-2005 and Sep-27-2009 IKONOS images were used. These two near-anniversary dates eliminate variation in plant phenology and focus our interest on tree physiological change. Moreover, the collection time was 19:04 GMT (12:04 local time) and 18:55 GMT (11:55 local time), respectively, which ensures similar sun angles and subsequently similar shadows cast by tree crowns and other tall objects. This is important because IKONOS image is prone to shadow effect. Satellite collection angles are also similar.

A fuzzy supervised classification using all the 4 multispectral bands (blue, green, red and near-infrared) was conducted in ERDAS with both the Minimum Distance and the Maximum Likelihood decision rules. Signature separability evaluation suggested that this four-dimensional feature space created the highest separability among classes. Among the four bands, the near-infrared band played the key role. It accounted for 50% of the average separability among the signatures. 9 classes were defined: Salt Damaged Conifers, Healthy Conifers, Medium-Healthy Conifers, Broadleaf Trees, Grassland, Water, Road, Construction, and Bare Soil. Broadleaf species account for a very small portion of vegetation in the Lake Tahoe Basin. They were thus classified as one class. The selection of signature for "Salt Damaged Conifers" class was especially careful. 2009 field survey plots with extensive salt damage were targeted for selecting the 2009 signature of this class. Tree GPS coordinates and orthorectified 1-m resolution panchromatic band were used as ancillary data to help locate salt damaged tree crowns in the 4-m resolution multispectral image. Extracted individual pixels of such damaged tree crowns on the multispectral image were merged as the final signature for this class. As for the 2005 classification, I used 2006 field survey plots with extensive salt damage as reference to select the signature for the "Salt Damaged Conifers" class on the 2005 multispectral image. The 2006 ground reference data is the earliest available data set. I noticed that there was very little change in the salt-damaged plots even between 2006 and 2009. So using 2006 field data to help selecting this particular signature for 2005 classification should be fine. Except this signature, all other signatures were visually selected directly from the imagery of each year. As for the "Healthy Conifers" class, I chose the tree crowns with very high greenness or NDVI as its signature. As for "Medium-Healthy Conifers", a polygon area of a general healthy and dense conifer stand was chosen as the signature. As shown in the result, few pixels were classified as "Healthy Conifers", and most were classified as "Medium-Healthy Conifers". Given the above method of selecting the signatures for these two classes, "Healthy Conifers" (with very high level of greenness) and "Medium-Healthy Conifers" are merged into a single "Healthy Conifers" class. 3 best classes were assigned to each pixel according to the selected decision rule. Output consisted of a 3-layer classification image and corresponding distance file. Layer 1 contained class values for the best classification,

layer 2 with the second best, and so on. Thus each pixel had three colors representing three classes it belonged to, making up a RGB color classification map.

Fuzzy classification takes into account that there are pixels of mixed make-up. For example, a 4-m multispectral pixel of IKONOS may contain half tree crown and half bare soil. Fuzzy classification makes it possible to obtain information on what different constituent classes can be found in a mixed pixel. It also reveals that some classes might have certain similarity in the spectral constitution or overlap in the multidimensional spectral feature space. This is not strange for the four tree classes: Salt Damaged Conifers, Healthy Conifers, Medium-Healthy Conifers, and Broadleaf Trees. A signature separability test showed that Healthy Conifers class had least divergence from Broadleaf Trees, and so did Salt Damaged Conifers from Medium-Healthy Conifers, according to Jefferies-Matusita or Transformed Divergence measures. A fuzzy convolution tool in ERDAS was then operated to create a single classification layer by calculating the total weighted inverse distance of all the classes in a moving window of pixels using the output distance file. The center pixel in the window was assigned to the class with the largest total weighted inverse distance summed over the entire set of fuzzy classification layers. Classes with a very small distance value remained unchanged while classes with higher distance values might change to a neighboring value if there was a sufficient number of neighboring pixels with that class value and small corresponding distance values. Fuzzy convolution helps create a context-based classification to reduce the "salt and pepper" effect, and makes full use of the information in the multiple classification layers extracted by the fuzzy classification.

Both Minimum Distance and Maximum Likelihood decision rules were tried. The Minimum Distance rule produced lots of misclassifications. It classified a large amount of vegetated pixels as water. Maximum Likelihood method had a much better performance. Although it misclassified a small portion of water pixels as road or construction, there was no misclassification between vegetated and non-vegetated objects. Overall, Maximum Likelihood method had much better accuracy of classification than Minimum Distance. This is because Minimum Distance rule merely depends on the Euclidean spectral distance between the measurement vector for the candidate pixel and

the mean vector for each signature, while Maximum Likelihood method not only uses the mean vector of each signature but also takes the variability of classes into account by using the covariance matrix of the pixels in the training sample of each class.

Finally, post-classification change detection was conducted by subtracting 2005 classification image from that of 2009. A change map was generated; different colors were assigned to different types of change (Figure 4).

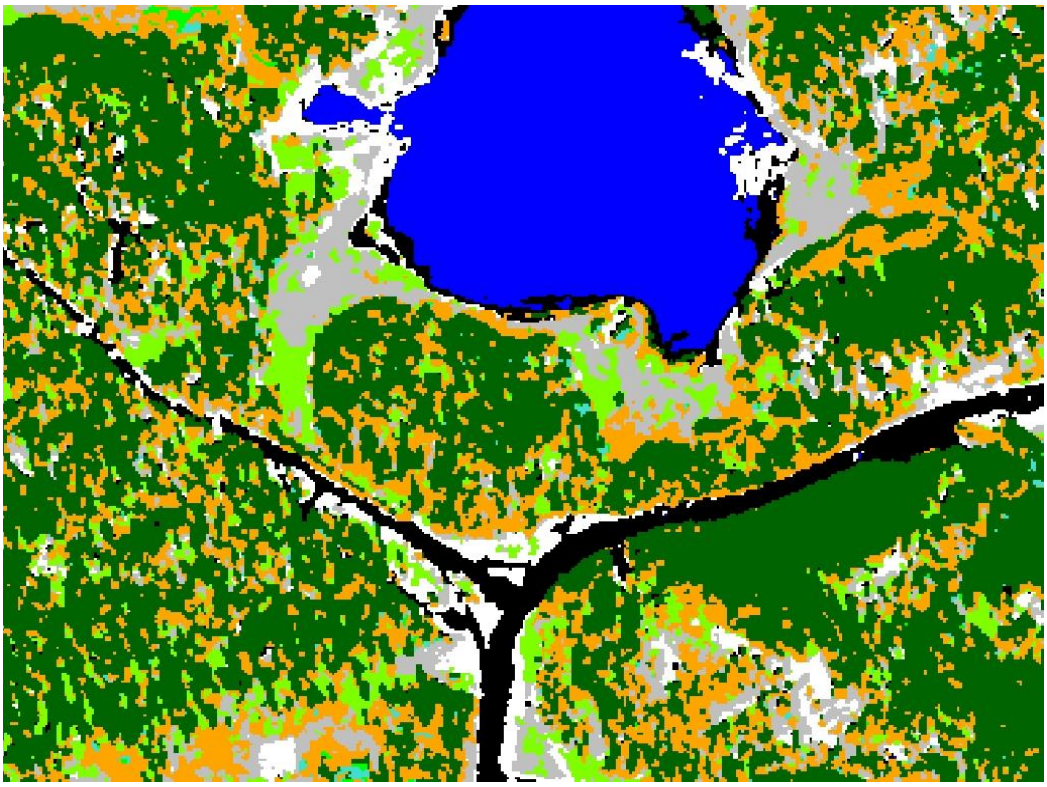

**(a)** Sep. 25, 2005 Classification

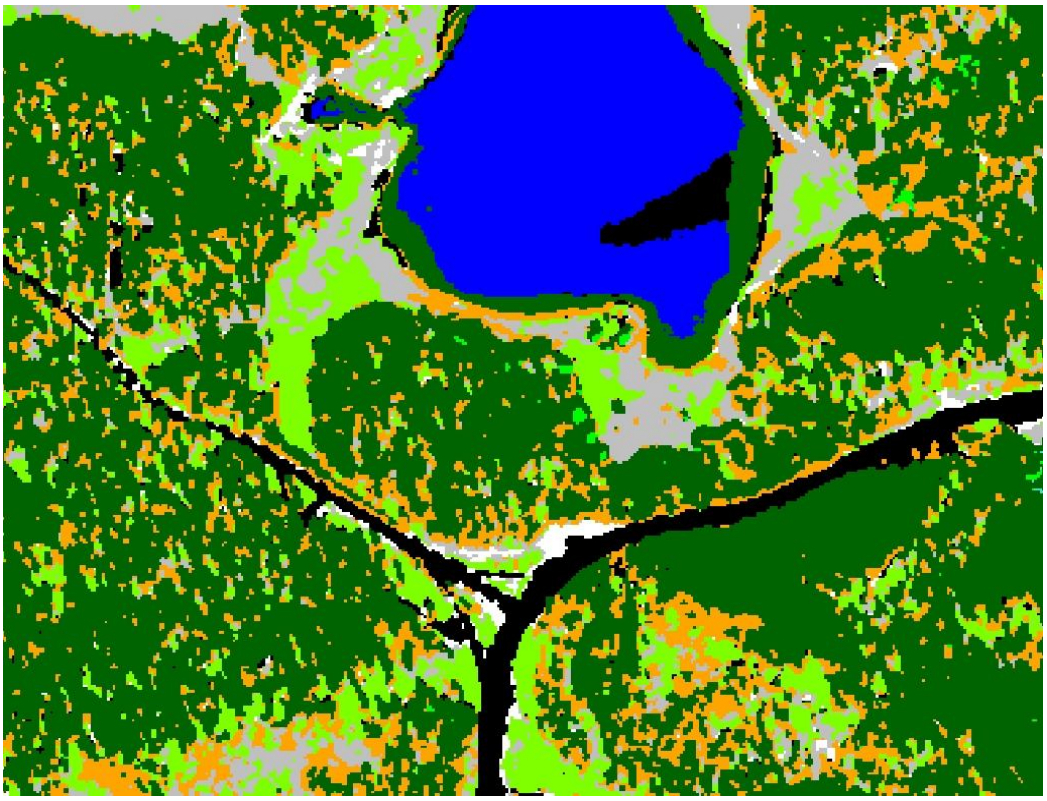

**(b)** Sep. 27, 2009 Classification

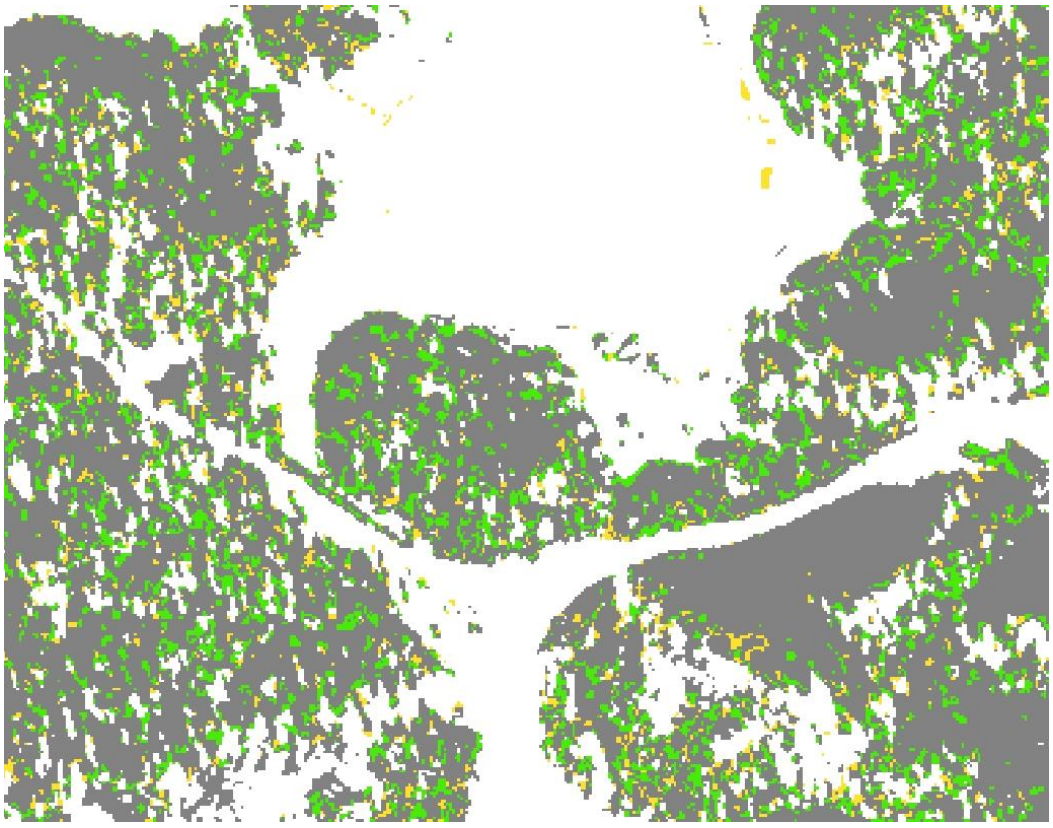

**(c)** Post-Classification Change Detection from 2005 to 2009

**Figure 4.** Multispectral fuzzy classification results of (a) Sep. 25, 2005 and (b) Sep. 27, 2009, and Post-Classification Change Detection result (c). (a) and (b) are the final single-layer classification images generated by fuzzy convolution after the 3-layer fuzzy classification. Orange color represents trees with damage; dark green color represents healthy trees; light green for grassland; gray for bare soil; blue for water; and black for road. Other minor classes cannot be seen in this scale. In (c), green color indicates change from unhealthy/damaged (in 2005) to healthy (in 2009); yellow indicates an opposite direction of change; gray means unchanged area with healthy trees. Other kinds of change are masked out by white color.

Results show that the classified salt-damaged trees disperse throughout the basin and their quantity is much lower than healthy trees. However, de-icing salt damage should only exist near roads according to field study. This suggests that tree crown mortality can be well extracted by classification but whether it is caused by de-icing salt or by other factors cannot be distinguished by classification. It means that the spectral characteristics of de-icing salt damage might not have significant difference from other kinds of tree crown damage, or the four spectral bands of IKONOS might not be appropriate or sufficient enough to capture the subtle variation in spectral response of different damage types. Nevertheless, the classification results are still informative. With post-classification change detection, a change map with distinct change types was generated. The map (Figure 7(c)) tells that from 2005 to 2009, there was deceased amount of damaged trees and increased healthy trees throughout the extent of IKONOS imagery (Nevada side of Lake Tahoe Basin). Apparently, much more trees had changed from being unhealthy to healthy than the opposite direction. This is consistent with the fact that there was a prolonged extensive draught before 2005 (from 1998 to 2003), and several years after the draught the forest has obvious regeneration and restoration.

# Chapter 3 Improvement of Ground Reference Data Collection

Different vegetation indices and change detection results are related to vegetation parameters (and their change) such as absorbed photosynthetically active radiation (APAR), leaf area index (LAI), canopy cover, and foliage biomass in varying ways. What these satellite-derived digital data can tell us about the real status of vegetation cannot be determined until they are calibrated with ground reference data about that vegetation. It is also important to calibrate different forms of remote sensing results (e.g. ΔNDVI & MKT

components) to a uniform ground reference data so that they can be interpretable and comparable. Ground reference data collection generally involves measuring the Diameter at Breast Height (DBH) and health status of each tree in the sampling plots or the overall canopy cover at plot level. This is what we did in the summers of 2008 and 2009, so did colleagues previously in 2006 and 2007. More sophisticated methods may include measuring Leaf Area Index (LAI) or Absorbed Photosynthetically Active Radiation (APAR) that are more closely related to the actual relative abundance and activity of green vegetation. This is the improvement that I have tried to make. There was no chance to conduct improved field method in Austrian forest; instead, this was done in the original study area Lake Tahoe basin in the USA. This is actually more helpful because of consistency and continuousness in the data, which facilitates analyses and comparison. For the original ground reference data, only an initial effort of using them to calibrate MKT change detection was made immediately after the fieldwork was finished. They were explored in more detail in the period of this Marshall Plan study. Thus both the new findings from original field data set and the recently improved field method and its results are presented.

## 3.1 Original Ground Reference Data and Its Utility

### 3.1.1 Original Ground Reference Data Collection

Based on the previous field data we have from related projects, our original ground reference data collection followed their way of mainly measuring DBH and health status of each tree in a plot. This information was compiled and transformed to healthy canopy cover for each plot. Each plot had a size of 30m × 30m and corresponds exactly to a pixel on Landsat TM image by virtue of the high precision Trimble GeoXT GPS. Relationships between remote sensing estimates and field measurements were thus straightforward.

The previous field-based project "Effects of De-icing Salts on Vegetation in the Lake Tahoe Basin" provides detailed field survey data (216 plots) on tree crown severity of salt damage and other agents such as insects and pathogens for 2006 and 2007. The plots are roughly 100ft × 100ft (30.48m × 30.48m) squares, which are very close to the size of 30-m Landsat TM image pixels, although they were not geo-referenced to the pixels. The

locations of all trees and plot corners were recorded by Garmin GPSMAP 60CSx GPS with precision over 1 meter. By overlapping those coordinates on Landsat image, 70 out of the 216 plots were observed to have more than 80% overlap with Landsat pixels. Those plots were chosen to be resurveyed as discussed later.

From Aug. 15, 2008 to Sep. 10, 2008, we surveyed 35 field plots, including 1347 trees. Each plot is a 30m × 30m square, exactly representing a single pixel selected from Landsat TM imagery. Each square was located on the field by the coordinates of four corners of corresponding pixel using sub-meter precision GPS (Trimble GeoXT GPS). All the trees with DBH>10 cm within the square were surveyed and tagged. We recorded coordinates (latitude and longitude) of the plot center, elevation, slope, number of trees, and canopy cover (measured with densiometer in four directions parallel to plot edges at the plot center) for each plot; and tree species, DBH, salt damage rating, needle damage rating, pathogen ID, disease severity, insect ID, insect severity, dieback, and overall tree health for each tree (see Table 3).

P2 =IF(C2="JP",(0.9488+0.0356*D2),IF(C2="WF",(1.2256+0.0299*D2),IF(C2="IC",(1.296+0.0256*D2),IF(C2="SP",(0.9906+0.0398*D2),0))))

| | A | B | C | D | E | F | G | H | I | J | K | L | M | N | O | P | Q | R |
|---|---|---|---|---|---|---|---|---|---|---|---|---|---|---|---|---|---|---|
| 1 | Plot No | Tree No | Species | DBH (cm) | Salt Damage Rating | Needle Damage Rating | Pathogen # ID | Disease Severity | Insect # ID | Insect Severity | Overall Tree Health | DIEBACK | Notes | Basal Area of Each Tree | Overall Basal Area | Crown Radius of Each Tree (m) | Canopy Area of Each Tree ($m^2$) | A |
| 2 | SHC-1F | 1 | JP | 18.2 | 0 | 0 | 0 | 0 | 0 | 0 | A | 1 | | 260.1553 | 14665.8 | 1.59672 | 8.0095368 | 8.009537 |
| 3 | SHC-1F | 2 | JP | 37 | 0 | 0 | 1 | 3 | 0 | 0 | C | 3 | | 1075.21 | | 2.266 | 16.131312 | 0 |
| 4 | SHC-1F | 3 | WF | 32.6 | 0 | 0 | 0 | 0 | 0 | 0 | A | 1 | | 834.6898 | | 2.20034 | 15.210009 | 15.21001 |
| 5 | SHC-1F | 4 | JP | 18.8 | 0 | 0 | 1 | 3 | 0 | 0 | C | 3 | | 277.5911 | | 1.61808 | 8.2252641 | 0 |
| 6 | SHC-1F | 5 | JP | 45 | 0 | 0 | 1 | 2 | 0 | 0 | B | 2 | | 1590.431 | | 2.5508 | 20.441026 | 0 |
| 7 | SHC-1F | 6 | JP | 38 | 0 | 0 | 1 | 3 | 0 | 0 | B | 2 | | 1134.115 | | 2.3016 | 16.642155 | 0 |
| 8 | SHC-1F | 7 | JP | 12.2 | 0 | 0 | 0 | 0 | 13,12 | 3 | DEAD | 4 | | 116.8987 | | 1.38312 | 6.0099325 | 0 |
| 9 | SHC-1F | 8 | WF | 31 | 0 | 0 | 8,2 | 1,1 | 0 | 0 | B | 2 | Resinosis and needle | 754.7676 | | 2.1525 | 14.555804 | 0 |
| 10 | SHC-1F | 9 | JP | 55.5 | 0 | 0 | 1 | 3 | 0 | 0 | A | 1 | | 2419.223 | | 2.9246 | 26.870938 | 26.87094 |

**Table 3.** Field data sheet of previous forest mortality survey conducted in the summers of 2008 and 2009.

In the summer of 2009 (Jun. 09 to Oct. 09), the above 35 plots of 2008 were resurveyed using the same method. In addition, 42 plots of 2006 and 29 plots of 2007 which have more than 80% overlap with Landsat pixels were re-located by GPS and were adjusted to correspond to those 30m×30m pixels. Trees outside of the pixel were excluded and only those in were re-surveyed. At the mean time, a small portion of trees that are in the pixel but are outside of the overlap area were not originally surveyed in 2006 and consequently were not re-surveyed in 2009. We suppose that such small portion of trees will not cause major change of the pixels. The dataset cannot be used to calibrate

single year vegetation indices, but they can calibrate change detection results as long as the majority of trees in the pixels were surveyed and they carry the main change information. This give us a chance to detect forest changes over a time interval longer than one year (e.g. from 2006 to 2009 and from 2007 to 2009).

### 3.1.2 Calibration Methods

#### 3.1.2.1 DBH-Canopy Cover Model

The first try of making use of these field data was carried out though a DBH-Canopy Cover allometric model and "Weighted Healthy Canopy Cover" equation. The allometric model estimates crown radius by DBH using a linear equation per species (Gill et al., 2000):

$$crrad = b_0 + b_1 DBH \tag{5}$$

where crrad is the crown radius and $b_0$, $b_1$ are the species-specific parameters. Crown area can be easily calculated from crown radius. This model was created based on Sierra Nevada conifer species which almost comprise all the Lake Tahoe conifer species except Jeffrey Pine, which is genetically related and very similar to Ponderosa Pine. So the parameters for Ponderosa Pine were used for Jeffrey Pine in my study. The nearly identical geographic location and ecological condition facilitates the use of this model. After canopy area of each tree was calculated, the qualitative measurement of health status of each tree in our field data was used to weight the raw canopy area and the overall healthy canopy cover per plot was derived:

$$HealthyCanopyCover = \sum A*100\% + \sum B*80\% + \sum C*30\% \tag{6}$$

Consequently healthy canopy cover change between different years was derived:

$$\Delta HealthyCanopyCover = \Delta \sum A*100\% + \Delta \sum B*80\% + \Delta \sum C*30\% + \sum (A + B)*5\% \tag{7}$$

where Healthy Canopy Cover is the estimation of healthy or effective portion of green area that a tree canopy actually has and can be recorded on the remote sensing images. A, B, C refer to the field measured health status of each tree and designate in the equation the canopy area of each tree belonging to these health status classes. $\sum A$, $\sum B$, $\sum C$ are the

sums of crown area of the trees in a plot belonging to the three classes, respectively. According to the forest pathologist who did the reading, A was assigned to a tree with >89% of the crown is healthy, B to approximately 60-89% healthy crown, C to <50% healthy crown, and D to dead trees. The last term with 5% is an estimation of normal tree growth rate for general healthy trees in three years, which was later substituted by a Potential Relative Increment of diameter model (PRI) (Equation 8) that was supposed to be less arbitrary and more accurate.

Equation 7 contains both quantitative (i.e. absolute tree death) and qualitative (i.e. health status change in living trees) aspects of field data. A decrease in $\sum A+\sum B+\sum C$ (without weighting) from 2006 to 2009 reflects the amount of trees that were alive in 2006 but dead in 2009 (marked as D or DEAD), that is, absolute tree death. The weighting method was used in consideration that DBH was not re-measured due to the fact that the minimal growth in DBH of the conifers in three years cannot exceed the amount of measurement error. In addition, even if DBH had been re-measured very accurately, the weighting method would have had to be used to derive canopy change information because health status can decrease (i.e. healthy canopy cover can decrease) while DBH increases or remains constant. Therefore, the change of tree health status including tree death was chosen as the indicator of total healthy canopy cover change. Even though there is inherent limitation when using partially qualitative field data to calibrate quantitative remote sensing change detection results, this method is novel in that I make use of both qualitative and quantitative change information and thus are able to calibrate change detection (based on vegetation indices) using tree health change (described by defoliation and discoloration) rather than using solely physical canopy cover change from measured tree death, on which many other studies were based. An improved relationship between change detection result and field data under this use will enhance the accuracy of calibration in our study.

When all the 42 plots surveyed in both 2006 and 2009 were used as calibration dataset, none of the three change detection results had significant relationship with the field data (NDVI $R^2$=0.21; MKT Greenness $R^2$=0.09; MSAVI $R^2$=0.08). This was ascribed to several factors:

(1) Original survey in 2006 and resurvey in 2009 were done by two different forest pathologists and the health statuses were assigned by visual estimation on the ground. There was inevitable difference in their visual estimations, especially between the statuses A and B, which were assigned to healthy trees and trees with minor damage. Change from A to B might only occur in part of tree crown (especially bottom because readings were taken from below tree crown) and not cause a significant change in remote sensing signature. For example, 92 of 132 trees in Plot D-123 were assigned health status B in 2006 but status A in 2009, which results in a huge healthy canopy cover increase, when Equation 7 is applied. However, none of the three vegetation indices show any significant change.

(2) Another issue with our field data is that we only measured tree DBH. Estimating crown radius/biomass from DBH by allometric models is inherently hampered by the variation in crown morphology associated with tree density, physiology, geography and many other factors. So, future field survey should include measuring crown radius directly or using radiometer to measure LAI or APAR that are more closely related to vegetation indices.

(3) Plot size: per-stand basis VS per-pixel basis? When designing the plots, we thought a 30m×30m plot could exactly represent a single pixel on Landsat TM image, and could be located by GPS. Pixel-size plot might be too small, thus too sensitive to the misregistration between Landsat images. Justice and Townshend (1981) suggests A=P(1+2L), P is pixel size and L is the positional accuracy of the geometric registration in terms of pixels. So 60×60m should be a better plot size for the Landsat TM data.

(4) Understory species and trees with smaller than 10cm DBH were excluded in the field survey. Moreover, the 42 plots used above were originally set up in 2006 without reference to Landsat pixel. They were re-adjusted to 30m×30m pixels by the 80% overlapping rule. A small portion of trees that were not surveyed exist in some pixels (see 3.1.1). Although we suppose that understory species and other

trees not surveyed will not constitute significant change in the time interval, they might have certain change actually but not used in the calibration. Thus bias might occur.

(5) We measured every tree (>10cm DBH) in a plot and canopy cover was derived by summing all trees' crown area regardless of canopy overlap, while satellite sensors can only sense the outer layer of canopy. The overall aboveground biomass will be inherently underestimated by optical sensors. Thus errors occur when using overestimated field data to calibrate underestimated remote sensing results. Direct LAI measurement on a plot basis, which will be discussed in section 3.2, is supposed to minimize such effects, because the LAI sensor measures the whole plot three-dimensionally and LAI itself takes into account foliage overlap.

(6) Numerous studies have shown that satellite-derived vegetation indices are optical measures of canopy greenness, a composite property of leaf chlorophyll content, leaf area, canopy cover and structure. However, vegetation indices have often been employed as proxies for individual, and often land-cover-dependent, vegetation attributes such as fractional canopy cover and LAI. These attributes as a portion of the composite canopy property, when used individually, are only moderately correlated with vegetation indices. Thus using vegetation indices to estimate these parameters separately is subject to error and uncertainty (Glenn et al. 2008).

Issues (1), (2), (3), (4), (5) are supposed to be solved if new ground reference data are collected using the modified field data collection method as described in section 3.2. Issue (6) remains an inherent limitation of optical remote sensing and worth notice in later statistical analyses.

To make better use of the current field dataset, each plot was examined with regard to the above issues and outliers were excluded in the regressions according to reasonable findings behind the plot data:

Plot C-100A is beside the highway. Vegetation indices and field data showed opposite change directions. According to issue (3), misregistration between Landsat images can be around 1/2 pixel which could cause pavement content to increase in pixels on one side of the road and decrease on the other side between different years. As it can be seen in the change images, there is an obvious zigzag effect along highways: pixels with drastically positive change values are always accompanied by pixels with negative change values opposite to them. Plots under this effect significantly influence the regression. Thus plot C-100A was deleted. Other plots under this effect include: W-5, W-6 and D-6.

Plot D-123 was deleted as explained in issue (1). 92 of 132 trees in this plot were assigned health status B in 2006 but status A in 2009. Vegetation indices, however, all showed decrease. It could be more possibly caused by difference in estimates by two different surveyors rather than real health change. H-107 is also under this effect.

E-1030 was deleted because there are only 13 conifers in the plot. Most of the ground surface is covered by deciduous species such as willow, snowberry, ribes and amelanchier whose canopy varies much more dramatically compared to conifers and they were not surveyed. Other plots under this effect include E-114, D-3 and W-8.

D-20 has a lot of young white firs, whose canopy would have grown a lot. However, trees with DBH <10cm were not included in the survey. Thus field data cannot reflect this growth. It was deleted.

H-111 plot is across two pixels. Only half of the trees of each pixel were surveyed. This kind of plot is not reliable, because even if the pixels values are averaged, other trees that cause the average change of the two pixels might be outside of the plot. In other words, trees surveyed might not be able to reflect the overall change of two pixels. Thus, this plot was excluded.

After scrutinizing all the plots' data for unwanted variations, 30 plots were finally used in the regressions. The coefficient of determination showed significant improvement.

The R squares rose to 0.67, 0.61, and 0.46 for ΔNDVI, ΔMKT Greenness and ΔMSAVI, respectively. The scatter plot for ΔNDVI is shown below. Others are shown in Figure 3.

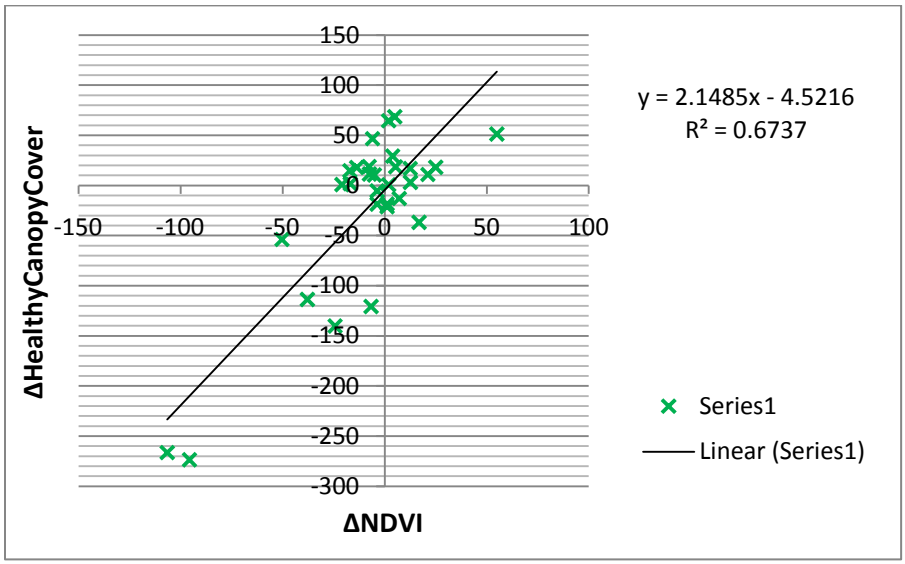


**Figure 5.** Relationship between Δ Healthy Canopy Cover derived by Equation 7 and ΔNDVI derived from 2006 and 2009 anniversary Landsat TM images. ΔNDVI was rescaled by 1000.

#### 3.1.2.2 DBH-Foliage Biomass Model

To check if the afore mentioned problems were related to the DBH-Canopy Cover linear model, another allometric model "DBH-Foliage Biomass" was tried. Comparison was made to see which model is more accurate and whether canopy cover or foliage biomass is more closely related to remotely sensed indices. DBH-Foliage Biomass equations were chosen from the Comprehensive Database of Diameter-based Biomass Regressions for North American Tree Species (Jenkins et al., 2003). In this database, different forms (e.g. linear, logarithmic and polynomial) of allometric regression equations for different tree components (e.g. foliage, stem, roots) that are species-specific are summarized.

In this database, there is no foliage equation for Jeffrey pine, so the equation of its close relative Ponderosa pine was used. For the same reason, Western White pine was treated as the same as Sugar Pine. There are two equations for Lodgepole Pine. The average of the results of the two equations was used. There is no foliage equation for

Incense Cedar. So I used the average result of six equations for its two close relatives: Northern White cedar and Western Red cedar.

Regressions showed that using foliage biomass data to calibrate change detection did not make any improvement. ΔNDVI consistently performed much better than the other two change detection methods. Figure 6 shows the scatter plot using ΔNDVI.

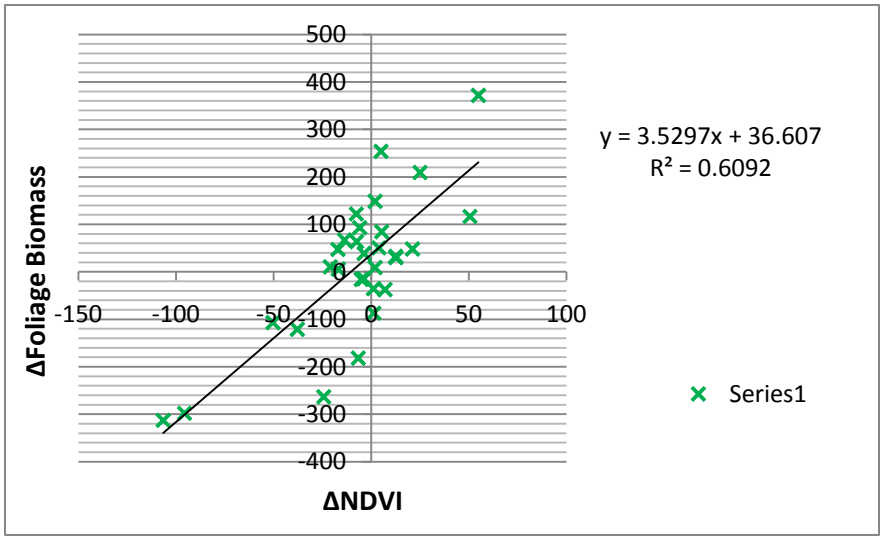


**Figure 6.** Relationship between Δ Total Healthy Foliage Biomass derived from USFS database of DBH-based allometric models and ΔNDVI derived from 2006 and 2009 anniversary Landsat TM images.

#### 3.1.2.3 Growth Rate Model

To examine if the estimated growth rate of 5% used in Equation 7 is appropriate or not, published growth rate models that are species, age, and/or site specific were tried to be incorporated into the equation instead of the constant rate.

Initially, I attempted to use the growth equations from Dolph (1988) who developed site-dependent growth equations for predicting periodic basal area increment for young-growth mixed-conifer species in Sierra Nevada. The very similar geographic location and species composition was appealing. However, these equations require lots of site-specific parameters. Our field data don't include two necessary parameters: site index and crown ratio. Even though this paper provides an optional equation without site index, missing crown ratio is still a problem. Crown ratio is dependent on tree age and height. It is not

good to use an average value for a species. Otherwise the error incurred will outweigh the improvement of including other site parameters. Thus this attempt was given up.

In this situation, another diameter increment prediction model requiring only DBH at the starting point was used. It is called Potential Relative Increment (PRI) of Diameter (Bragg 2001). It was derived by fitting a power function to the maximum 5 year Actual Relative Increment (ARI) data to provide an equation for PRI, which is the maximum possible growth rate within a 5-year period for species at a given DBH:

$$\mathrm{PRI}=b_1\mathrm{DBH}_t^{b_2}b_3^{\mathrm{DBH}_t} \quad (8)$$

where $\mathrm{DBH}_t$ is current tree DBH; $b_1$, $b_2$, and $b_3$ are species-specific regression coefficients. Multiplying the PRI by the current DBH and then by 3/5 yields optimal periodic diameter growth in 3 years.

The tree species used in Bragg's paper do not include all the species in my study. Thus a representative species was chosen for fir, pine and cedar, respectively, by genus and subgenus relationship. Balsam Fir was chosen to represent genus Abies such as White Fir and Red Fir. Parameters for them are: b1=2.64702; b2= -0.407958; b3= 0.960849. Red Pine was chosen to represent subgenus Pinus including Jeffrey pine, Lodgepole pine and Ponderosa Pine. Parameters are: b1=3.29264; b2=-0.358137; b3=0.952945. Eastern white pine represented subgenus Strobus: Sugar Pine and Western White Pine, with parameters: b1=3.856766; b2=-0.553002; b3=0.979675. Northern white-cedar represented Incense-cedar, with parameters: b1=1.92589; b2= -0.41927; b3= 0.959847. These growth equations were used to derive new DBHs for trees in 2009 which were then used in the DBH-Crown Radius allometric model (Equation 5) to derive new crown areas. Then Equation 6 was used instead of Equation 7 to calculate new healthy canopy cover per plot for 2009. Difference between 2006 and 2009 was the healthy canopy cover change.

Regression was run with the new healthy canopy cover change data. Disappointedly, result showed a slight decrease of R square (Figure 7) compared to that using a constant estimated growth rate. This is probably because Equation 8 calculates the maximum

diameter growth without considering competition, disease and other site-specific parameters. Therefore, overestimation occurs. It shows that the increase in canopy cover of living trees, without considering other factors, from 2006 to 2009 calculated by this method ranges from 3% to 20% for all plots. The average rate is 10%. This coincides with the estimated growth rate 5% used in Equation 7 for some plots. Most plots have larger growth rates as they might be overestimated by Equation 8.

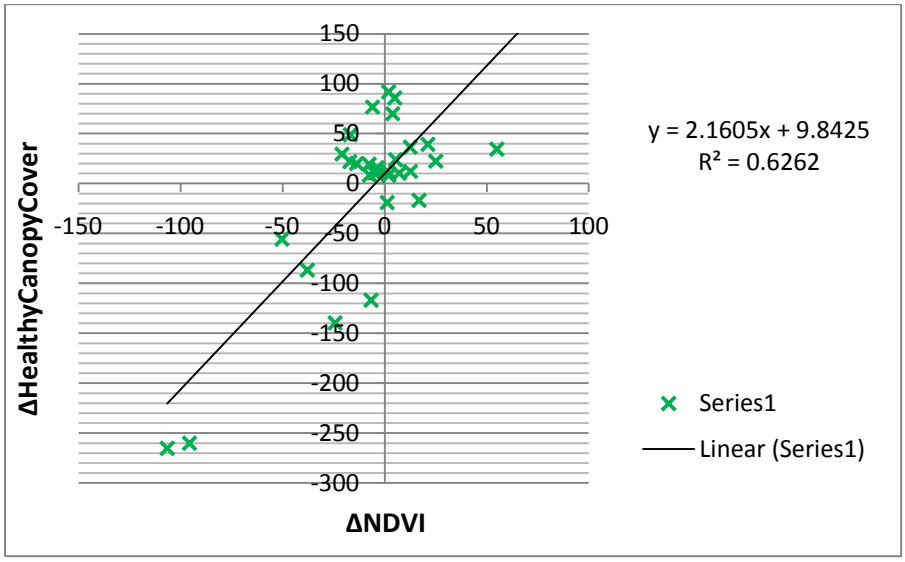


**Figure 7.** Relationship between Δ Healthy Canopy Cover (derived by Equation 6 with the use of the growth rate Equation 8) and ΔNDVI (derived from 2006 and 2009 anniversary Landsat TM images). ΔNDVI was rescaled by 1000.

Using a model always has certain limitation. In the future, to accurately measure growth rate, timber core samples should be obtained from living trees and their DBH growth in the past can be retrieved by measuring the width of annual growth rings.

#### 3.1.2.4 Canopy Cover Measured by Densiometer

Densiometer is a very simple equipment for measuring canopy cover at plot level. Canopy cover is estimated by counting how many of the 96 equal-spaced points/squares in a concave or convex mirror surface are occupied by canopy and multiplying the number by 1.04. It is efficient but also subject to much variation caused by operating error, including variation in measurement direction and position, failure of leveling, sun shining, and error in counting sky/canopy occupancy on the small grid. However, since

this data is already included in our field dataset, it is worth comparing it with the DBH-derived canopy cover data.

Densiometer was only used in the 2008 and 2009 field survey where the canopy cover for 35 pixel-size plots was recorded at the plot center facing four directions, in addition to tree-based DBH and health status measurements (see section 3.1.1). Different from the 2006 and 2009 dataset (42 plots) used in calibrating change detection results (section 3.1.2.1 to 3.1.2.3), these 35 plots were originally designed to be pixel-size squares corresponding to Landsat TM pixels. Thus, they can be used to calibrate single-image derived vegetation indices, though they are not suitable for calibrating change detection because of the short one-year time interval.

To make a comparison, the DBH and tree health status data measured at the same time for these 35 plots were used to calculate single-year healthy canopy cover by Equation 6. Regression with densiometer-measured canopy cover data against single year vegetation index performed significantly better than that with DBH-derived healthy canopy cover (Figure 8). This again, suggests that the modeling approach is not as sound as direct plot-level measurements. This also predicts that there will be an improvement with the modified ground reference data collection method which will be discussed in the following section.

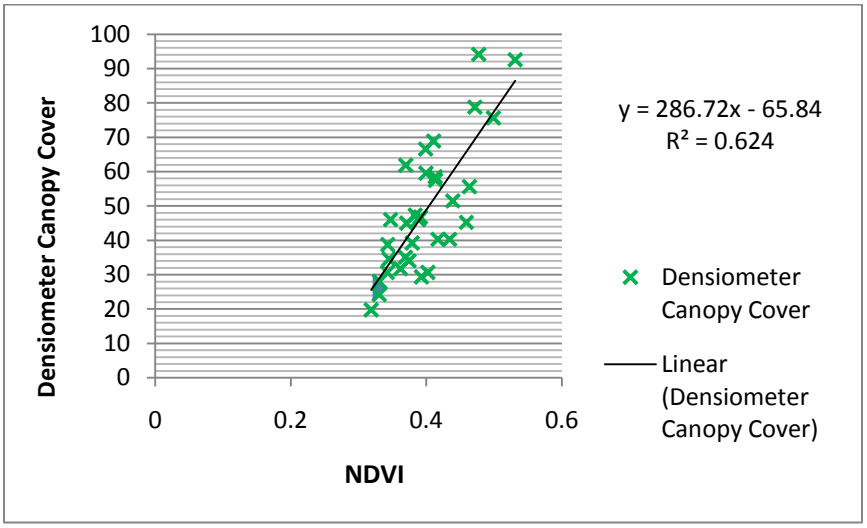


**(a)**

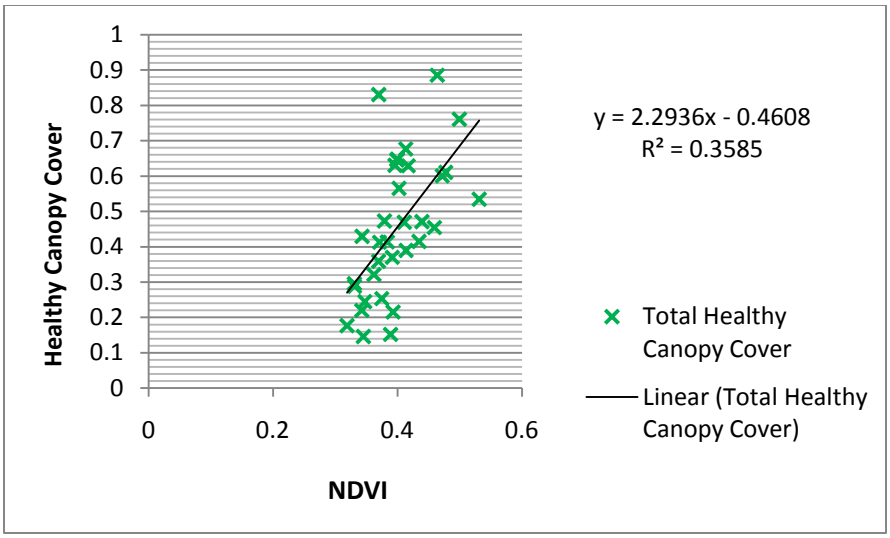


**(b)**

**Figure 8.** Relationship between NDVI (derived from 2009 synchronous Landsat TM image) and (a) Canopy Cover measured by densitometer, (b) Healthy Canopy Cover derived by Equation 6 with 2009 field data.

## 3.2 Improved Ground Reference Data Collection Method

The previous method involves collecting field-surveyed tree health data at two different points of time and using the change to calibrate remote sensing change detection. The thorough exploration of that data set in the above section suggests that a modified field method is necessary. However, when the following improved method is designed, I cannot go back to the past to make a correction. The only choice is to apply it to collecting single-year ground reference data due to the project schedule. Thus, instead of calibrating change detection results, I have to calibrate single-year remote sensing result (e.g. vegetation index) with the new ground reference data set. It is reasonable to calibrate vegetation index to field-measured canopy cover, foliage biomass or LAI for the concurrent year and generalize the relationship to other years for the same study area. Change information will be derived by differencing calibrated data sets of different years.

The new method was designed in August, 2010 involving measuring Leaf Area Index (LAI) directly using LI-COR LAI-2000 Plant Canopy Analyzer. This equipment calculates Leaf Area Index and other canopy structure attributes from diffuse radiation measurements made with a “fish eye” optical sensor. Its optical sensor is filtered to reject

radiation above 490 nm, which minimizes the influence of radiation scattered by the foliage. Measurements made above and below the canopy are used to determine canopy light interception in five angular bands about the zenith (0.0 - 12.3°; 16.7 - 28.6°; 32.4 - 43.4°; 47.3 - 58.1°; 62.3 - 74.1°). The light interception information is then used to compute LAI with a model of radiative transfer in vegetative canopies. The measured LAI directly represents the actual abundance and status of live vegetation on a plot basis. Thus it is more closely related to vegetation indices than canopy cover is.

Sampling plots were selected based on the following criteria:

(1) There must be an opening with bigger than 60-m diameter near each plot for above canopy readings. Since forest canopy is tall and we only have one LAI-2000, the above reference readings have to be made in an open site. A big enough opening makes sure that no radiation from adjacent vegetation is sensed by the lowest angle (74.1°) of the LAI-2000 sensor. A short distance to the sampling plot ensures that I can run between the opening site and plot in a short time, because this equipment requires measurements to be made without direct sun shine which means the only possible time is before sunrise and after sunset for the Lake Tahoe Basin, where there is rarely overcast weather.

(2) Plots should contain as little understory vegetation as possible. One reason is that understory vegetation is usually hard to measure because low plant height often makes plants below the lowest view angle of the equipment or blocked by uneven ground surface. Another reason is that pure conifer plots enhance the relationship between LAI measurements and remote sensing data by minimizing noise caused by potential different responses of LAI-2000 sensor and satellite sensor to variation in plant spectral properties. If there is inevitable understory vegetation, then measurement should be taken at the ground level to include understory vegetation. Since remote sensor captures everything in the pixel, it is thus reasonable to measure all vegetation in the plot as well.

(3) Plots should make a long enough gradient of tree density range from low to medium to high, so that the regression against remote sensing vegetation indices will be more robust.

(4) Plots should vary in species composition so that the field data is more representative for the whole study area.

(5) Plots should be distributed at different elevations and with different slopes and aspects so that the data is more representative.

Eight 60m×60m plots were found and surveyed for testing. Each plot comprises 4 corresponding Landsat TM pixels. Pixel corners and centers were located and marked by flags. A 90 degree azimuth view cap was used, so that unwanted objects including me were blocked from the sensor. The 90 degree view also facilitated the sampling design as follows. Ten measurements were made for each pixel, including 2 reference readings at the open site, 4 below canopy measurements at four pixel corners, and 4 at the center of pixel facing four corners. The estimated view distance of LAI-2000 is around 20m. So, 8 below canopy readings should fully comprise the pixel and let some overlap for minimizing noise (Figure 9).

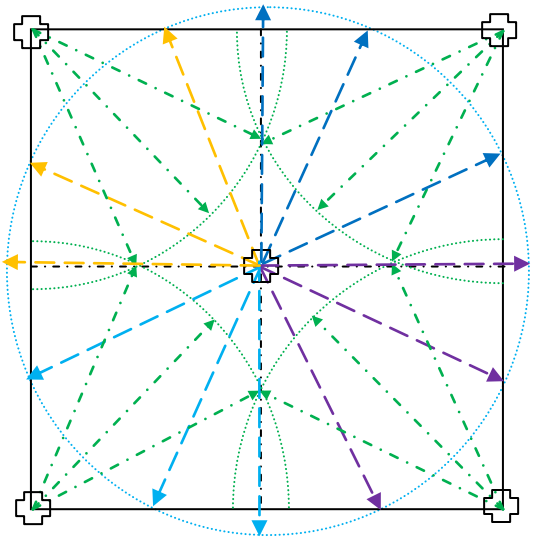

**Figure 9.** Sampling design for each pixel. The square is a 30m×30m pixel. 4 below canopy measurements are made at the four pixel corners (the 4 green 90 degree fan-shaped sectors). At the center of pixel, 4 below canopy measurements are made facing four corners (the 4 different color 90 degree fan-shaped sectors starting from the center).

The most critical and challenging part of this field work was the very limited measurement time and to find plots with big enough opening nearby so that it is feasible

to run between the opening and plot. Overcast sky is the best condition because when the direct beam of the sun is shining on foliage, scattered radiation is significantly increased and thus the below canopy readings are increased, resulting in underestimates of LAI. Unfortunately, there is rarely such weather in the Lake Tahoe Basin. It is always sunny in the summer and fall. Therefore, measurements can only be taken when the sun is near the horizon, where a nearby hill shades the measurement site. Even so, the time for measurement was very limited. In the morning, there was only 45 minutes maximum time before the canopy was illuminated and in the evening about 55 minutes.

In three days, we collected LAI data for eight 60m×60m plots, including 32 Landsat pixels. The NDVI values for these 32 pixels were extracted to predict the corresponding LAI values in the regression. The result was very encouraging (Figure 10). The coefficient of determination was much higher than using any of previous datasets. This proves that LAI measurement using LAI-2000 is reliable and the sampling design in the above trial was successful. This method should be extended for collecting more LAI data and for future study.

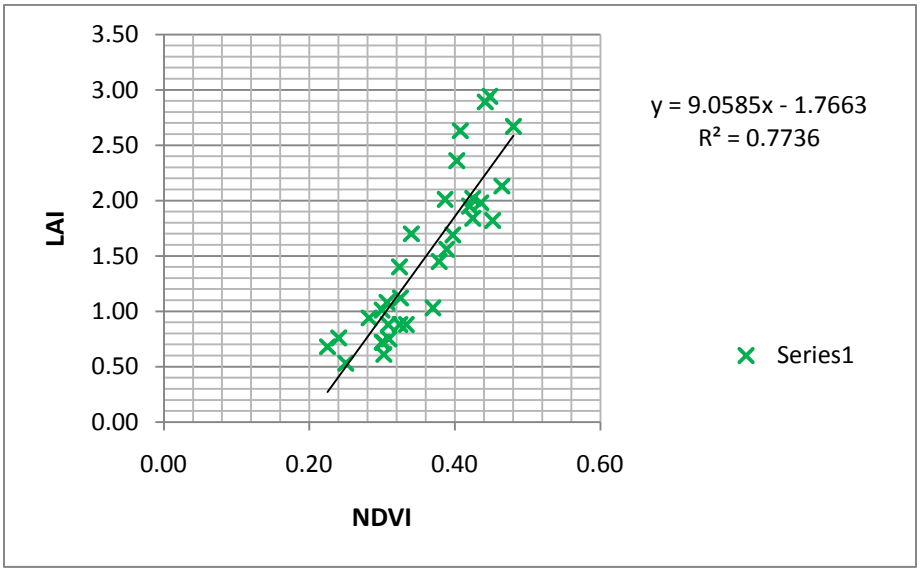


**Figure 10.** Relationship between LAI (measured by LI-COR LAI-2000 Plant Canopy Analyzer) and NDVI (derived from synchronous Landsat TM imagery).

Besides, it is worth mention that another method measuring Absorbed Photosynthetically Active Radiation (APAR) was also tried out before using the LAI-

2000 Plant Canopy Analyzer. The equipment I used was LI-COR LI-185A quantum/radiometer/photometer, with a Lambda quantum sensor (Lambda Inst. Corp.) calibrated to LI-185A. It measures photosynthetically active radiation (PAR) in the 400-700nm waveband. The unit of measurement is microeinsteins $m^{-2}sec^{-1}$. I used it to measure PAR under full sun radiation in open area and PAR after absorption under tree canopy in forested area. Their difference is thus APAR. APAR can be further transformed to LAI. APAR also directly represents the actual abundance and status of live vegetation and is closely related to vegetation indices.

However, this experiment failed because the quantum sensor was a line sensor. It actually only samples the portion of the canopy that lies between the sun and the sensor. Even a shift of leaves by mild wind makes the readings vary. Only under thick shadow of canopy the reading can be stable. This linear technique requires large and dense measurement grids in order to get useful estimates of LAI in forest where gaps exist within single tree canopy and between canopies. This is time consuming and limited by the quick variation in sun angle and radiation. In contrast with the LAI-2000 which measures LAI on the plot basis by virtue of its five-angle fisheye view, the data from LI-185A quantum sensor will be hard to represent the real leaf area index of a whole plot, but just the by-chance measured portion of canopy (very limited cluster of leaves) in between the sensor and sun. So the random error can be high even if I made measurements in 12×12 grid with 10-m interval.

# Chapter 4 IKONOS Image Preprocessing and Change Detection

## 4.1 Image Acquisition

In 2009, we purchased one new-collect IKONOS image for Sep. 27, 2009 and five archive images for the following dates: Aug. 10, 2001, Jul. 19, 2002, Aug. 10, 2003, Sep. 25, 2005 and Aug. 04, 2006. They encompass a buffer of approximately 2~4 km adjacent to the main highways traversing the east shore of Lake Tahoe, with a total coverage of 277 $km^2$ for archival imagery and 102 $km^2$ for new-collect imagery.

Only recently I noticed some errors and inappropriate parameters of the data. First, Rational Polynomial Coefficient (RPC) files of 2001, 2003 and 2005 images were missing, orthorectification of these images had to be suspended. Second, Dynamic Range Adjustment (DRA) was on for all the images which rendered them useless for our study because the spectral information was altered permanently in this process. Third, Cubic Convolution interpolation method was previously chosen for image resampling. I now find that Nearest Neighbor method is more appropriate for the purpose of this study. Fourth, IKONOS imagery has a virtue of 11-bit data depth, but we ordered ordinary 8-bit data. From these mistakes, previous IKONOS images have to be discarded. Reworking of all the previous orders has been processed by the courtesy of GeoEye. A new complete 11-bit dataset with proper parameters has been received. These important IKONOS parameters are worth clarification here.

First, Rational Polynomial Coefficients (RPCs) are the 3D approximation of the physical camera model of the satellite sensor. RPC files are the necessary for orthorectification. It is illustrated in detail in the following section.

Second, Dynamic Range Adjustment (DRA) is only appropriate for visual inspection of the image. It is a two step process that includes color correction and contrast enhancement. It results in visually-appealing imagery. However, as DRA alters the spectral information of satellite imagery and the original spectral data cannot be retrieved, it is not intended for spectral analysis and/or classification. This study requires original spectral information of the 4 multispectral bands. Thus, DRA should be off for the IKONOS images.

Third, resampling method should be carefully selected. Resampling is needed when projecting the raw satellite image onto a specific datum of a coordinate system or when pixels have to be re-arranged in the process of registration or orthorectification. Different resampling algorithms determine in different ways the spectral values that should be assigned to each pixel of the projected raster image. Cubic Convolution uses the values of sixteen pixels in a 4×4 window to calculate an output value for the center pixel with a cubic function, whereas Nearest Neighbor method uses the value of the closest pixel to

assign to the output pixel value. These two methods are distinct. Each has pros and cons. Careful comparison is needed. Nearest Neighbor transfers original data values without averaging them as the other methods do; therefore, the extremes and subtleties of the data values are not lost. This is an important consideration when discriminating between vegetation types (e.g. classification) or pixel-based change detection. But it introduces a small spatial error into the newly registered image. The image may be offset spatially by up to 1/2 a pixel, causing a jagged, blocky or stair stepped effect around diagonal lines and curves if there is much rotation or scale change. Cubic Convolution produces a smoother result with much less geometric error and at the same time keeps the mean and standard deviation of the original data much better than other interpolation methods (e.g. Bilinear Interpolation) do. Cubic Convolution shows its advantage when interpolating continuous data such as elevation surface (i.e. DEM). But it has to alter the original data values, which becomes a disadvantage when keeping the original value is considered to be more important than interpolating unknown values.

As for IKONOS image generation, raw intrinsic panchromatic and multispectral imagery (0.82m and 3.2m at nadir) was spatially resampled to 1 and 4 m, respectively, and was georeferenced to map coordinate system using either a Cubic Convolution or a Nearest Neighbor interpolation algorithm. Based on the above comparison, for the purpose of this study, I managed to get all the IKONOS images reworked by GeoEye with Nearest Neighbor resampling method in order to keep the original spectral information in the first place.

As for image processing such as orthorectification as shown in the next section or re-projection to different coordinate systems, Nearest Neighbor is also chosen for its better radiometric reliability, especially when the preprocessed multispectral images are to be used for spectral analysis and/or classification. Only when the IKONOS panchromatic image is processed for visual analysis such as tree crown delineation, or resample a DEM, Cubic Convolution will be used for better geometric accuracy and visual quality.

Finally, 11-bit data was obtained instead of the 8-bit data. The enhanced radiometric resolution has already shown noticeable uplifting effect during the classification process

as discussed in Chapter 2. Change detection results derived from this data will be helpful for statistically isolating road-related effects on tree crown mortality from other confounding factors.

## 4.2 Orthorectification and Change Detection

Raw satellite images usually contain geometric distortion due to terrain relief and tilt of the sensor and the inherent perspective projection of the image. Orthorectification is the process of transforming raw imagery to an accurate orthogonal projection, thereby removing the distorting effects of tilt and terrain relief. As illustrated in Figure 11, if the distance between A' and B' equals that between D' and E', the unequal lengths of line segments "ab" and "de" on the raw image (right) caused by relief displacement will be corrected to be equal on the resulting orthoimage (left). The product of orthorectification process is orthoimage, in which ground features are displayed in their true ground position. It combines the image characteristics of a photograph with the geometric qualities of a map.

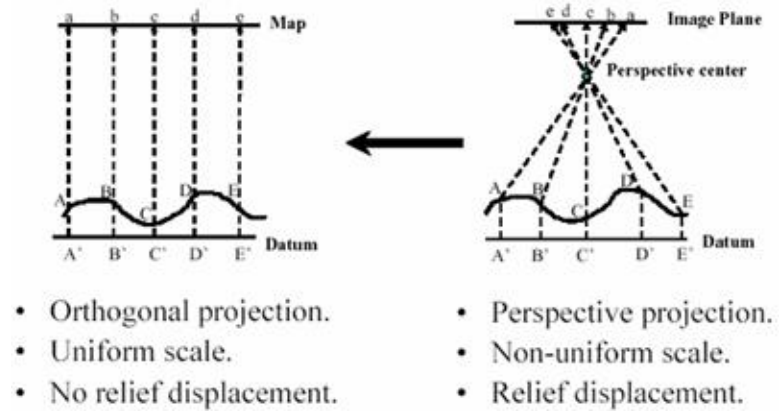


**Figure 11.** The illustration of orthorectification process. The graph is from Okeke (2006).

Different from Landsat TM imagery, which have been processed to Level 1T (i.e. terrain corrected) by incorporating ground control points, while also employing a Digital Elevation Model (DEM) for topographic accuracy, IKONOS images purchased from GeoEye have been processed only to Geo level by standard geometric correction with a 15 meter CE90 accuracy. Terrain effect is apparent in these images. However, this is an

Ortho Kit Bundle product which supplies Rational Polynomial Coefficients (RPC) files with all the images. This enables users having little familiarity with the IKONOS sensor physical model to perform orthorectification by the RPC model with only a DEM, or with additional GCPs to correct biases left by RPC model. RPCs express the relationship between object space (points on the ground) and image space (pixels in the image), that is, ground-to-image geometry. PRCs determination involves using the physical camera model to generate a 3D grid of points conveying information about the line-of-sight vectors passing through a large number of pixels in the Geo image, followed by least squares estimation of the rational polynomial function coefficients to fit this 3D grid (Lutes, 2004).

With the RPC files, I have a chance to independently orthorectify these IKONOS Geo-level images to high quality orthoimages. Orthorectification has been performed with two commercial remote sensing softwares: ENVI and ERDAS IMAGINE.

ENVI 4.7 has two orthorectification tools for IKONOS imagery: "Orthorectify IKONOS" and "Orthorectify IKONOS with GCPs". The former provides generic RPC orthorectification using RPC and DEM but without GCPs. Since biases or errors still exist when computing RPCs, the results of generic PRC correction need to be post-processed with a registration using GCPs. Alternatively, the original RPC correction model can be refined with a 0 or 1st order polynomial adjustment using GCPs and then the refined model can be applied to orthorectifying the data in one step. This is how the latter tool of ENVI and the "Geometric Correction" tool of ERDAS work. In the beginning, I thought the ENVI "Orthorectify IKONOS with GCPs" tool needed manual input of GCP coordinates and elevation before I discovered that GCP coordinates from reference image or map could be exported to the "GCPs Selection" tool box automatically by the "Pixel Locator" tool. Thus a two-step approach combining generic RPC orthorectification and image-to-image registration was taken. In the first step, terrain effect was eliminated in the resulting RPC-orthorectified image but it still had certain horizontal offset in X and Y coordinates compared to standard DOQ, due to a lower degree of accuracy of the rational polynomial camera model than the physical camera model. In the second step, a 0 or 1st order (affine transformation) polynomial

correction was applied to eliminate this offset using GCPs from reference image by the "Image-to-Image Registration" tool.

Later, orthorectification was also performed in one step by the ENVI and ERDAS. Resulting image was free from terrain effect and horizontal error. However, comparing the two approaches, I discovered that even though the two-step approach virtually had very similar result to that of one-step, they were not identical. The one-step approach is theoretically more reasonable. The following graph illustrates their difference.

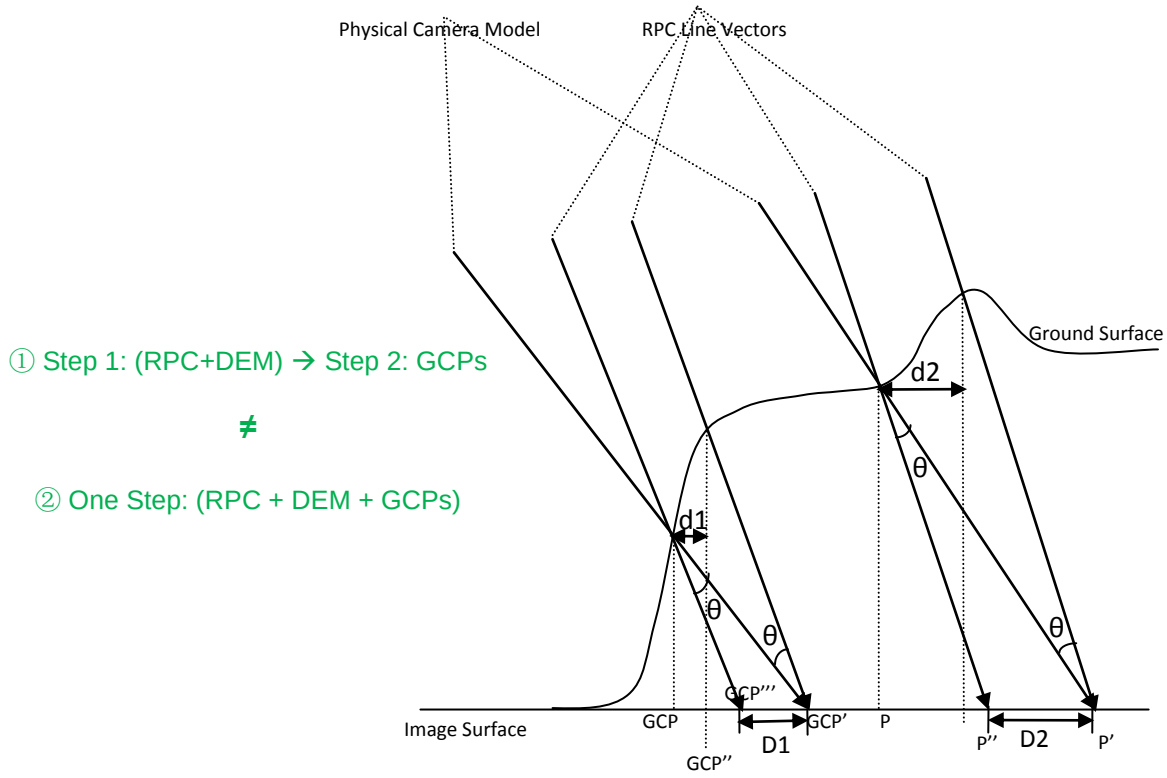


**Figure 12.** Assuming a 0 order polynomial transformation (simple shift to both image x and y coordinates) in both orthorectification methods, method ② works by shifting GCP' (uncorrected pixel) to GCP''' with distance D1 followed by projecting GCP''' to GCP (corrected or real position) using RPC model and DEM; method ① works by first projecting GCP' to GCP'' using RPC and DEM and then shifting GCP'' to GCP with distance d1. D1 ≠ d1, because of the variation in topography. Moreover, the effect of GCPs location on the correction of other pixels depends only on elevation for method ② (bias=|D2 - D1|; D1 and D2 are proportional to elevation) because RPC bias angle θ is the same for small ground region and image surface is level; whereas for method ①, the bias in correcting other pixels depends on slopes where GCPs located, as well as elevation because of uneven ground surface even though θ keeps the same (bias=|d2 - d1|; d1 and d2 are determined by elevation and slope).

In addition, the ENVI "Orthorectify IKONOS with GCPs" tool needs manual input of a constant Geoid offset if DEM data is in orthometric height such as the normally used NAVD88 vertical datum. ERDAS geometric correction tool makes an improvement on this issue. It not only follows the above illustrated one-step theory but also automatically adjusts in real-time any vertical datum mismatch between DEM and the model. It converts orthometric height value of every pixel to ellipsoidal height (Orthorectification requires the ellipsoid height for each pixel). The input of a single Geoid offset value for the whole study area in ENVI is not as sound as calculating geoid offset for every pixel as ERDAS does, because geoid offset varies from place to place.

Moreover, ENVI help and tutorial files wrongly interpret the meaning of "geoid offset". ENVI help says geoid offset is the "difference between a spheroid mean sea level (used in most available DEM data) and the constant geopotential surface known as the geoid", and "the RPC coefficients are created based on geoid height". Actually, there is no much difference between mean sea level and geoid. The separation between mean sea level and the geoid is referred to as (stationary) ocean surface topography, which varies globally in a range of $\pm 2$ m. Thus, geoid offset is not the difference between geoid and mean sea level, but it is the difference in height between the geoid and a reference ellipsoid such as WGS84, GRS80 or Clarke1866. Most DEM data contains elevation that is above mean sea level and is usually referenced to geoid-based vertical datum such as NGVD29 and NAVD88. This kind of height is called orthometric height, versus ellipsoidal height that is above the ellipsoid (e.g. WGS84 ellipsoid). RPC coefficients are created with respect to ellipsoid. Therefore, geoid offset value is used to transform orthometric height that is often used in DEM to ellipsoidal height that is required in RPC orthorectification.

This misinterpretation confuses users. I contacted ENVI customer service and they agreed such an error and created a bug report as said in following email: "I have to agree with your assessment of the descriptions of Geoid offsets in the ENVI Help and RPC tutorial. I have created a documentation bug report on this. It is CR58995 for future reference."

Based on the above findings, ERDAS was chosen as the final orthorectificaion tool. Before orthorectification started, initial effort was taken to update the elevation data and ground reference sources to the best available. First, I found that the 10-m resolution Tahoe DEM data from the Lake Tahoe Data Clearinghouse was actually not updated for a long time. It came from the DLG data source with 20 and 40 feet contours (1979-1998). No new elevation, enhancement, or any additional information has been included, as said in its metadata. Thus its high resolution does not imply any improvement. On the contrary, National Elevation Dataset (NED) from USGS National Map Seamless server uses newer data sources (from 1999 to 2001). In addition, data corrections were made in the NED assembly process to minimize artifacts, perform edge matching, and fill sliver areas of missing data. NED artifact removal greatly improves the quality of the slope and shaded-relief that can be derived from the elevation data. Since elevation data is crucial for orthorectification and DEM-derived slope and shaded-relief data are needed in the topographic correction and later statistical analyses of topographic effect on road-related tree crown mortality, NED data was acquired to substitute for Lake Tahoe Data Clearinghouse DEM.

In addition, 20 GCPs in the common coverage area of the five IKONOS images were collected using Trimble GPS in May by a lab assistant from the University of Nevada Reno. I inspected these GCPs. They have very good agreement with RenoCarson 1-feet orthoimage, their difference/offset is within 1.5m. Since the RenoCarson 1-feet orthoimage is announced to be within 1-feet accuracy and the Trimble GPS had within 1.5m real-time accuracy, I think that both these GCPs and the orthoimage have good quality. In comparison, the offset between GCPs and old DOQ or NAIP imagery is 3-5m. This suggests that their geometric accuracy is lower, which is also in accordance with NAIP's announced 6-m accuracy. Thus, the GCPs collected by Trimble GPS are quite reliable.

Finally, a full database of reference orthoimages and GCPs for orthorectifying IKONOS has been constructed, including 20 GCPs collected in May 2010, RenoCarson2007 1-feet orthoimages (upper part of Lake Tahoe NV side),

Carsoncity2008 0.3-m orthoimages (middle and lower part) and NAIP 2009 (middle and lower part) (Figure 13a).

For the 2009 IKONOS image, 12 GCPs were selected from the above sources. The solved geometric correction model had a total RMS error of 0.1899 m. For the 2005 image, 10 GCPs were selected from the above sources. The total RMS was 0.2124. Nearest Neighbor was chosen as the resampling method as discussed in section 4.1. The orthorectified 2005 and 2009 images show a geometric offset (simple x and y shift) of less than ¼ pixel for multispectral image. Thus the accuracy of registration between them was around 1 meter.

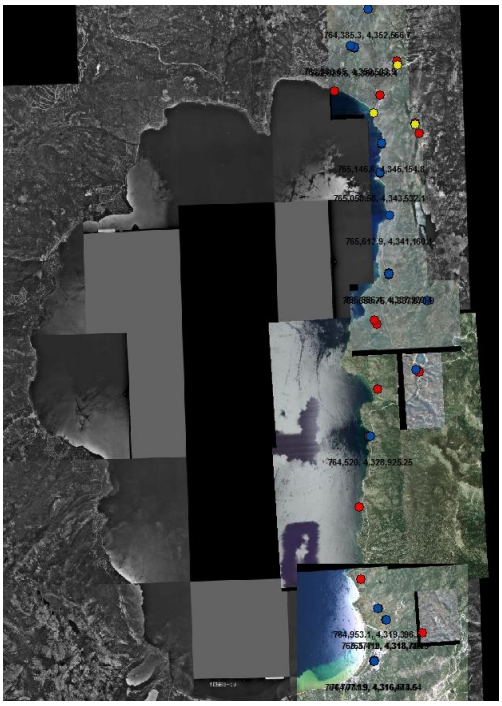

(a) Multiple best available reference sources

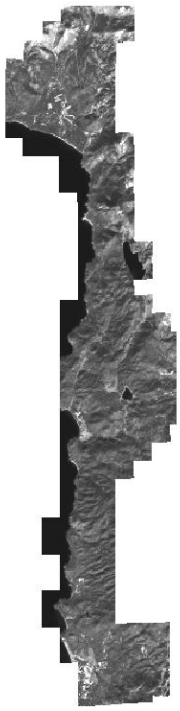

(b) Orthorectified panchromatic band

(c) Before orthorectification

(d) Orthorectified multispectral bands

**Figure 13.** Orthorectification process including reference data preparation (a) and output orthoimages (b) and (d). Difference can be seen between raw image and orthorectified image when (c) and (d) are overlapped.

NDVI images were generated from 2005 and 2009 orthorectified IKONOS multispectral bands. The difference image was also calculated (i.e. NDVI Differencing). They are shown in Figure 14. At this point, a thorough pixel-based change detection analysis using IKONOS data has not yet finished. It is out of the scope of this research assignment. The following NDVI difference map is the initial effort. IKONOS data has already shown its usefulness in the post-classification change detection (Chapter 2). Further use of IKONOS data will be necessary for fine-scale statistical analysis of road-related effects on tree crown mortality.

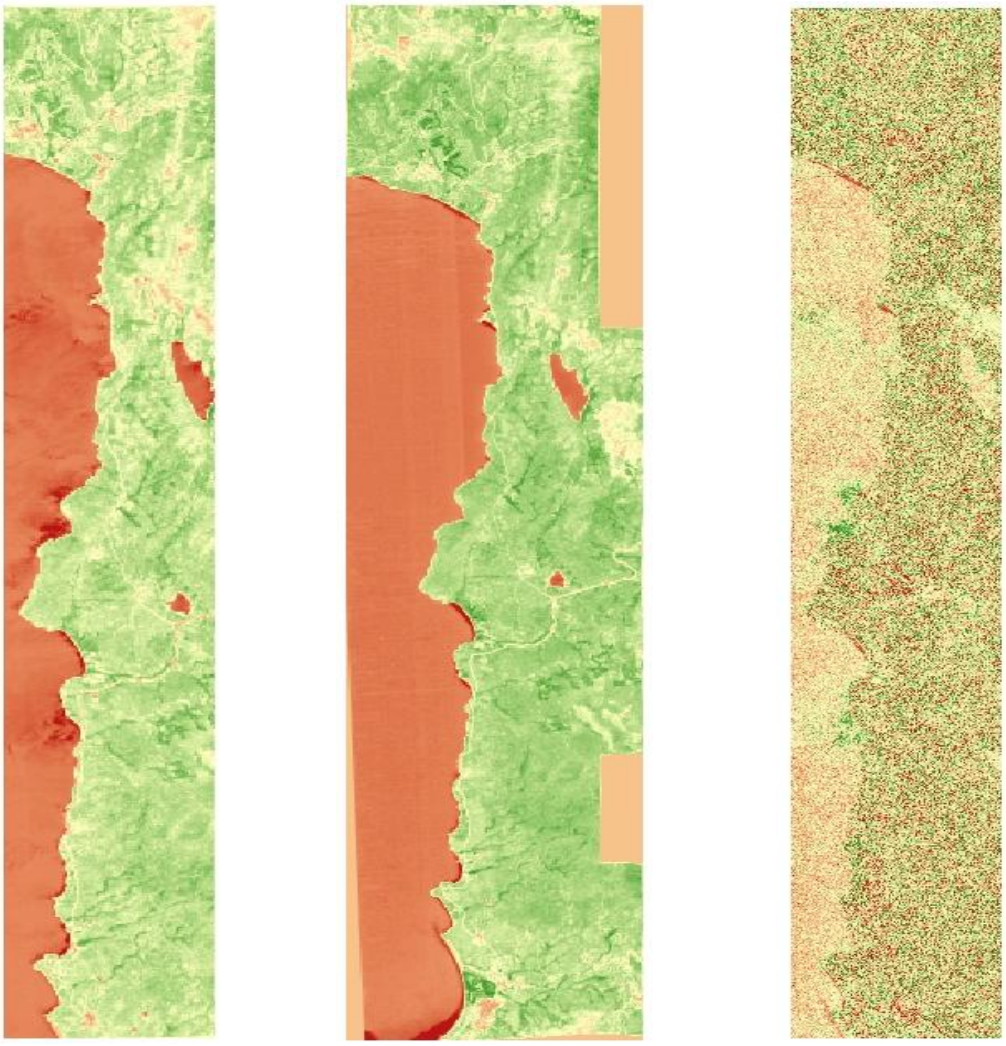

(a) 2005-09-25 NDVI (b) 2009-09-27 NDVI (c) NDVI Differencing

**Figure 14.** NDVI images derived from orthorectified IKONOS multispectral bands for Sep. 25, 2005 (a) and Sep. 27, 2009 (b). (c) is the difference image from 2005 to 2009.

# Chapter 5 Other Findings on Remote Sensing Methods

## 5.1 Improvement on Atmospheric Correction

### 5.1.1 Modification of Atmospheric Normalization Method

Atmospheric normalization is an important step before change detection. It eliminates unwanted change information caused by variation in atmospheric condition, sun radiation and other environmental conditions. I took an approach of using spectrally invariant features or so-called radiometric ground control points (RGCP) to calibrate a regression

equation between reference image and the image to be normalized. Previously I had rule of thumb that the September 18, 2008 scene should be selected as the reference to which scenes of all other years will be normalized. This was just because the 2008 imagery was the latest at that time. In this method, the selection of RGCPs had been especially careful. I tried using the whole water area of Lake Tahoe as spectrally invariant features, but the resultant normalized images showed strong overcorrection for land features. The reason was that RGCPs should include not only deep water bodies but also invariant land features such as bare soil, roads, large rooftops, parking lots, sand, and large rock outcrops, to ensure a long enough spectral gradient. In 2009, such 30 spectrally invariant feature plots (15 water bodies and 15 land features) were surveyed in field and corresponding pixels were chosen as RGCPs.

This method worked when some images before 2008 (e.g. 2005-10-12 and 2006-09-29 images) were normalized to the 2008-09-18 image. However, when it came to the 2009-09-21 image, the direction of normalization should be changed. The 2008 image should no longer be the reference. Key & Benson (2005) suggest that the scene less clear—the one with less transmittance—will be the one corrected and will become the independent variable in regression analysis performed later. Usually, this scene will exhibit brighter reflectance over dark targets, such as lakes, compared to values from the same targets in scenes with greater transmittance. Relative difference in transmittance can be determined quantitatively by comparing pixel reflectance sampled over dark targets. Lower transmittance also appears to decrease contrast, compared to scenes where the air is clear. The most affected bandwidths include the visible Bands (1, 2, and 3), so base comparisons on those bands to enhance differences. Band 1 is most influenced by atmospheric factors, so use it when comparing single bands. Compare bands between scenes individually as grayscales, in false-color combinations, or by their histograms. The scene with less transmittance should show less variance in the histogram and a shift to the right or brighter region. By observation, band 1 of 2008 has brighter reflectance of lake pixels; its minimum reflectance value of dark object is 0.057, bigger than 0.052 of 2009; its mean reflectance value 0.086 is also larger than 0.084 of 2009; and it also has smaller Standard Deviation which suggests decreased contrast or variance compared to that of

2009. Based on the above criteria, 2009-09-21 image is determined to have higher transmittance than that of 2008 and thus should be selected as reference.

As shown in the Figure 15, 30 spectral invariant pixels were used as RGCPs. The regression line shows that these 30 RGCPs represent a full range of spectral gradient from dark object to bright object. The coefficient of determination ($R^2$) or R is also very high. This suggests a high quality of these RGCPs. Coefficients from the regressions were applied to 2008 image so that atmospheric variation was canceled out (normalized) between 2008 and 2009 scenes. Change detection was performed on these normalized images thereafter.

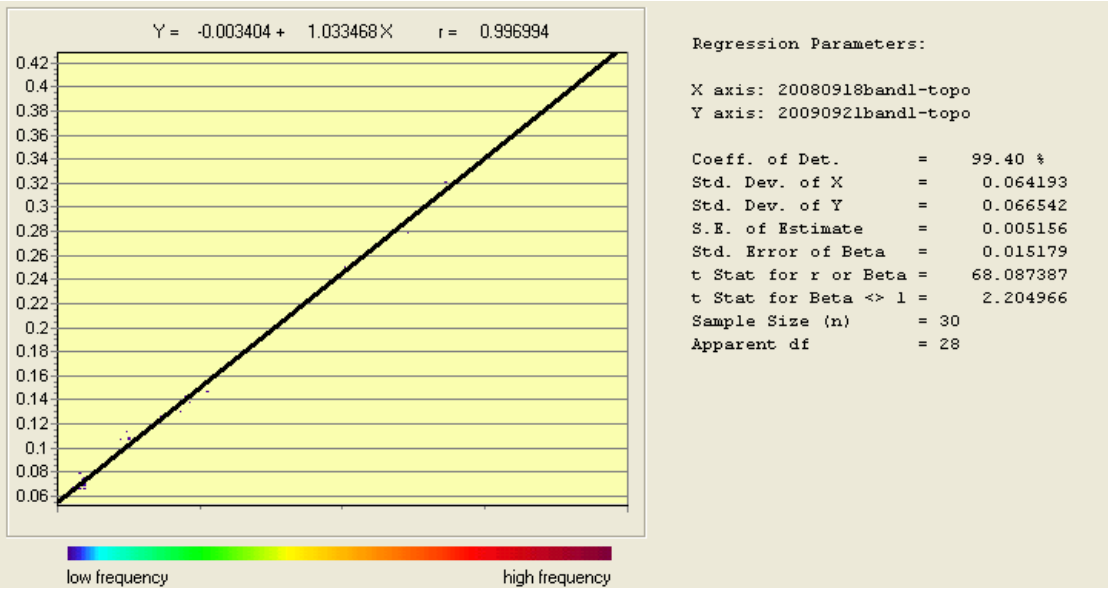


**Figure 15.** Image-to-image regression in IDRISI using the 30 spectral invariant pixels (RGCPs) as mask (small black dots along the regression line). Slope and intercept are to be used for atmospheric normalization.

### 5.1.2 Absolute Atmospheric Correction using ENVI FLAASH Module

Previous relative atmospheric correction was good for change detection purpose. However, when it comes to calibrating single year image derived vegetation indices, it is important that atmospheric noise can be eliminated so that remote sensing indices can be better related to field-collected real vegetation information. Absolute radiometric correction provides such a means.

Once I realized that the first decade of 21 century is coming to the end but most reference papers related to this subject that I had read were from last century. Unconsciously, I follow the well-know methodologies that are still useful but, to some degree, becoming antiquated. Due to limited computer technology and immature development of commercial remote sensing software, previous studies often times rely on relative radiometric correction to reduce atmospheric effects, without the need of knowing atmospheric properties that are difficult to acquire. Dark-object subtraction and image-to-image radiometric normalization are perhaps the most often used relative radiometric methods. Image-to-image radiometric normalization method using *spectral pseudo-invariant features* has been introduced as used in my study. Dark-object subtraction techniques assume that there is a high probability that there are at least a few pixels within an image which should be black (0% reflectance). Because of atmospheric scattering, remote sensing imagery records a nonzero DN value at these supposedly dark-pixel locations for a certain spectral band. Subtracting such a nonzero DN value from the particular spectral band can thus remove the first-order atmospheric scattering effect, or *haze*. The key is how to extract this DN value from the digital data. A simple and standard method is based on examining the lower portion of DN frequency histogram to select a non-zero small DN value of which there is a sharp increase in the number of pixels; or simply the minimum pixel value of the histogram is selected. This method allows histogram adjustment to achieve band-to-band normalization, which is referred to as single-image normalization using histogram adjustment in Jensen (2005). The limitation of this standard dark-object subtraction technique is that DN values selected for haze removal for the bands of a multispectral imagery may not conform to a realistic *relative* atmospheric scattering model. This lack of conformity may cause the data to be overcorrected in some or all of the spectral bands, and the spectral relationship between the bands will not be correct. Chavez (1988) developed an improved dark-object subtraction method by incorporating a user-selected relative scattering model (e.g. Rayleigh or Mie models, or so-called power law models in the paper) to predict the haze values for the other spectral bands from the starting haze value (decided by histogram method) of a selected band. The improvement is that the computed haze values for the multiple bands are wavelength-dependent and correlated to each other according to the

selected relative scattering model. Even so, the initial selection of a starting haze value by the histogram method is subject to the same uncertainty as other dark-object subtraction method, and influences the subsequent selection of relative scattering model. Overall, such methods are only effective in adjusting atmospheric scattering effect, especially for visible bands (TM 1, 2, 3) but cannot correct for atmospheric absorption, especially in longer wavelength bands (TM 4, 5, 7).

For example, the full radiometric correction and matching method described in Collins and Woodcock (1996) paper, to which my project tries to compare, was actually a combination of image-to-image radiometric normalization (which is similar to my method discussed previously) and band-to-band normalization using relative scattering model and dark-object subtraction (Chavez, 1988). As said, such methods cannot perform beyond the capability of a relative radiometric correction. When extracting vegetation information from a single image and calibrating it with ground reference data, it is essential that atmospheric effects can be corrected as much as possible. At this point, absolute radiometric correction is preferable; so that we can turn the plain digital count values recorded by a remote sensing system into meaningful scaled surface reflectance values which can then be compared or used in conjunction with surface reflectance information obtained by other means from anywhere on the earth.

Commercial remote sensing software has developed quickly by incorporating latest atmospheric correction methods. One example is ENVI's Fast Line-of-sight Atmospheric Analysis of Spectral Hypercubes (FLAASH), developed by Spectral Science, Inc., in collaboration with the U.S. Air Force Research Lab and Spectral Information Technology Application Center personnel. This is an automated absolute atmospheric correction module that corrects images for atmospheric water vapor, oxygen, carbon dioxide, methane, ozone, and molecular and aerosol scattering using a MODTRAN 4+ radiative transfer code. The two most important user inputs are the selections of an aerosol model and an atmospheric model for aerosol retrieval and water vapor retrieval, respectively, based on the information of image bands themselves.

This tool was tried with the Aug. 23, 2010 Landsat TM image. Since Landsat TM imagery has no appropriate wavelengths for water retrieval for each pixel, an atmospheric model was selected with the input of a constant column water vapor amount for all pixels in the image. However, column water vapor amount is difficult to obtain for the Lake Tahoe area. In this situation, the standard column water vapor amount for the selected "U.S. Standard" atmospheric model was used. Aerosol retrieval is possible using the Landsat TM band 3 at 0.66 um wavelength and band 7 at 2.22 um wavelength. Several aerosol models were tried. Results showed that when "Urban" model was selected, the retrieved visibility was 15.6229 km, which was very close to the reported visibility 10 mile (16 km) for Lake Tahoe area on the date of Aug. 23, 2010 from NOAA weather forecast. Other input parameters are not discussed here. The output corrected image using "U.S. Standard" atmospheric model and "Urban" aerosol model was used to calculate NDVI and this new NDVI was used in the regression to predict LAI measured by LAI-2000 Plant Canopy Analyzer (see Chapter 3). Results did not show any improvement over the regression using the same LAI data but NDVI derived from raw DN image (as in section 3.2). I examined the FLAASH-corrected image and found that the near-infrared band 4 was overcorrected. It had lower minimum brightness than red band 3 before correction because of mainly water vapor absorption in band 4 and mainly aerosol scattering in band 3. But after correction, band 4 became having higher minimum brightness than band 3. This was most possibly caused by not knowing the actual column water vapor amount for the Lake Tahoe area at the specific time. The input of a constant column water vapor amount was very likely improper.

To cope with this problem, I plan to use synchronous MODIS Terra level-1B 1-km resolution calibrated radiance data to retrieve water column amount for the time same as the Landsat TM imagery collection time. MODIS imagery provides rich spectral bands and high spectral resolution that fulfill ENVI FLAASH module's requirement to perform water vapor retrieval. If it is successful, the retrieved column water vapor amount will be used as a complement to Landsat's spectral limitation.

## 5.2 SCS+C Radiometric-Topographic Correction

Lake Tahoe Basin has very complex topography. There is no more than 20% flat ground surface. Elevation ranges from 1897 m at lake level to 3320 m at Freel Peak. Radiometric-topographic effect (i.e. radiometric distortion of recorded signal caused by slope and aspect) is prominent on the remote sensing images. Previously, two common used radiometric-topographic correction methods: Cosine Correction and C-Correction were tried. I found the latter had significant improvement over the former one which showed obvious overcorrection. The algorithm of C-Correction is:

$$\rho_H = \rho_T \left(\frac{\cos \theta z + c_k}{IL + c_k}\right) \quad (9)$$

where $\rho_H$ is the reflectance of a horizontal surface (topographically corrected); $\rho_T$ is the reflectance of an inclined surface; IL is the illumination value of every pixel on the image, computed by a self-built illumination model using NED and information of sun elevation angle and azimuth angle at the time of image collection; $\theta z$ is the sun zenith angle; $c_k = b_k/m_k$, where $m_k$ and $b_k$ are the slope and intercept of the regression line for band k using the following empirical-statistical regression model:

$$\rho_T = b_k + m_k IL \quad (10)$$

If the whole image is used to derive $c_k$, the method is called general c correction; if a specific land cover type is used to derive $c_k$, the method is called specific c correction. Specific c correction can significantly enhance the accuracy of topographic correction for the concerned forested surface. I used the forest type from the National Land Cover Data (NLCD) as the mask for the above regression model to derive specific C.

As an additional effort, SCS+C topographic correction method was tried out. The *Sun-Canopy-Sensor* (SCS) model was developed by Gu and Gillespie (1998). It normalizes sun-canopy-sensor geometry instead of sun-terrain-sensor (STS) geometry on which many traditional topographic correction methods such as Cosine Correction and C Correction are based. SCS method normalizes the sunlit area within a pixel without changing the sun and sensor positions or the orientation, geometry, and structure of the

canopy. It is thought to be a more appropriate framework for topographic correction in forested areas. However, even SCS model also overcorrects the radiance for some terrain, because it does not characterize diffuse radiation properly which is a problem common with earlier methods. Soenen et al. (2005) made a modification to the SCS model to better characterize diffuse irradiance by introducing a semi-empirical moderator C to account for diffuse radiation. This is very similar to the way in which C-Correction made the improvement on the earlier Cosine Correction. The formula for SCS+C correction is:

$$\rho_H = \rho_T \left(\frac{\cos \alpha \cos \theta z + c_k}{IL + c_k}\right) \quad (11)$$

where all the parameters are the same as in equation 9 except that α is the terrain slope as the added parameter. IL (illumination) can also be written as cos(*i)*, where *i* is the incidence angle on each pixel defined as the angle between the normal to the pixel surface and the solar zenith angle. Without the parameter $C_k$ the above equation becomes the original SCS.

SCS method was also recommended by my advisor Dr. Schneider from the Institute of Surveying, Remote Sensing and Land Information. They have another modified version of SCS which incorporates the correction for diffusive radiation in shaded area in a sophisticated way. At this point, the simpler SCS+C method was tried. Since I already built the model for C-Correction, an easy modification was made by adding the parameter cos α. At present, no adequate ground reference data is available for checking the accuracy of the topographic correction made by SCS+C method. I tried to compare the regressions as in Figure 10 using NDVI derived from raw DN image to that derived from topographically corrected image to see the effect of the correction. However, the recently sampled LAI plots were mostly on flat surface for better accessibility and because there was very limited choice due to the plot selection criteria (section 3.2). The field data from flat plots cannot reveal any effect of the correction nor the difference between the two topographic correction methods. Although the C-Correction already showed to be very good, it is worth comparing it with SCS+C once suitable ground reference data is available.

## *Conclusion*

Based on the above findings, some informative insights are obtained for future research. First of all, a well-designed ground reference data collection is crucial for calibrating and validating remote sensing results. Fieldwork is usually time consuming and hard to be corrected afterwards. Thus a thorough feasibility study has to be made in advance so that a minimum input of fieldwork can sufficiently achieve the goal of connecting remote sensing results to real world information. In turn, an efficient remote sensing approach is aimed to minimize the need for inefficient field-based study. As for this study, measuring LAI on a plot basis by the LI-COR LAI-2000/2200 Plant Canopy Analyzer is obviously more optimistic than the tree-by-tree based attributes measurement. Secondly, the soil-adjusted vegetation indices are not necessary for characterizing forest health in the context of this study. Either NDVI or K-T (Tasseled Cap) indices is sufficient. Consequently, the MKT change detection method is suitable for this study and enables direct comparison with the previous remote sensing study on the same area. Post-classification change detection is a useful tool to extract explicit change information. Although it is qualitative and is not able to differentiate different types of mortality, it can be a quick guidance to understand the pattern of general forest mortality and the direction of all kinds of change. Next, IKONOS imagery provides necessary finer data than the Landsat TM imagery for the fine-scale analyses of road-related effects on tree crown mortality. After processed with improved image preprocessing methods such as relative or absolute atmospheric correction, topographic correction and orthorectification, the multiple-scale remote sensing data, together with refined change detection methods, are ready for further exploitation to finally accomplish the statistical analyses, and to establish a robust protocol for future efficient monitoring of tree crown mortality associated with roads.

## *Acknowledgement*

I thank the Austrian Marshall Plan Foundation for funding this research during my joint study at the University of Natural Resources and Life Science (BOKU), Vienna, Austria. I thank Dr. Werner Schneider for his attentive advising and warm hosting in the Institute of Surveying, Remote Sensing and Land Information (IVFL). I also thank Dr. Tatjana Koukal and all other members in this institute for their kind help and friendly communication with me. The BOKU University and IVFL institute provided necessities for doing this research. The Nevada Department of Transportation, USA funded the IKONOS images and other data used in this study.

## *References*

Baret, F., & Guyot, G. (1991). Potentials and limits of vegetation indices for LAI and APAR assessment. *Remote Sensing of Environment, 35*, 161-173.

Bragg, D. C. (2001). Potential relative increment (PRI): a new method to empirically derive optimal tree diameter growth. *Ecological Modeling, 137*, 77–92.

Chavez, P.S. (1988). An improved dark-object subtraction technique for atmospheric scattering correction of multispectral data. *Remote Sensing of Environment, 24*, 459-479.

Collins, J. B., & Woodcock, C. E. (1996). An assessment of several linear change detection techniques for mapping forest mortality using multitemporal landsat TM data. *Remote Sensing of Environment, 56*, 66-77.

Colwell, J. E. (1974). Vegetation canopy reflectance. *Remote Sensing of Environment, 3*, 175-183.

Crist, E. P., & Cicone, R. C. (1984). Application of the Tasseled Cap concept to simulated Thematic Mapper data. *Photogrammetric Engineering and Remote Sensing, 50*, 343-352.

Dolph, K. L. (1988). Prediction of periodical basal area increment for young-growth mixed conifers in Sierra Nevada. *USDA Research Paper PSW-190.*

Gill, S. J., Biging, G. S., & Murph, E. C. (2000). Modeling conifer tree crown radius and estimating canopy cover. *Forest Ecology and Management, 126*, 405-416.

Glenn, E. P., Huete, A. R., Nagler P. L., & Nelson S. G. (2008). Relationship between remotely-sensed vegetation indices, canopy attributes and plant physiological processes: what vegetation indices can and cannot tell us about the landscape. *Sensors, 8*, 2136-2160.

Gu, D., & Gillespie, A. (1998). Topographic normalization of Landsat TM images of forest based on subpixel sun-canopy-sensor geometry. *Remote Sensing of Environment, 64*, 166–175.

Huete, A. R. (1988). A soil-adjusted vegetation index (SAVI). *Remote Sensing of Environment, 25*, 295-309.

Huete, A. R., Jackson, R. D., & Post, D. F. (1985). Spectral response of a plant canopy with different soil backgrounds. *Remote Sensing of Environment, 17,* 37-53.

Jackson, R. D., & Huete, A. R. (1991). Interpreting vegetation indices. *Preventive Veterinary Medicine, 11,* 185-200.

Jenkins, J. C., Chojnacky, D. C., Heath, L. S., & Birdsey, R. A. (2003). Comprehensive Database of Diameter-based Biomass Regressions for North American Tree Species. USDA General Technical Report NE-319.

Jensen, J. R. (2005). Introductory digital image processing: a remote sensing perspective. Pearson Education, Inc. 310-322; 474-491.

Kauth, R. J., & Thomas, G. S. (1976). The Tasseled Cap-a graphic description of the spectral-temporal development of agricultural crops as seen by Landsat. *Proceedings, Symposium on Machine Processing of Remotely Sensed Data,* West Lafayette, IN: LARS, 41-45

Key, C. H., & Benson, N. C. (2006). Landscape Assessment (LA): Sampling and Analysis Methods. USDA Forest Service Gen. Tech. Rep. RMRS-GTR-164-CD. 2006.

Lutes, J. (2004). Accuracy Analysis of Rational Polynomial Coefficients for IKONOS Imagery. *Proceedings of ASPRS 2004 Conference*, Denver, May 23-28, 2004.

Okeke, F. I. (2006). Review of Digital Image Orthorectification Techniques. Department of Geoinformatics and Surveying, University of Nigeria, Enugu Campus, Nigeria. http://www.gisdevelopment.net/technology/ip/fio_2.htm.

Qi, J., Chehbouni, A., Huete, A. R., Kerr, Y. H., & Sorooshian, S. (1994). A modified soil adjusted vegetation index. *Remote Sensing of Environment, 48*, 119-126.

Soenen, S. A., Peddle, D. R., & Coburn, C. A. (2005) SCS+C: A Modified Sun-Canopy-Sensor Topographic Correction in Forested Terrain. *Ieee Transactions On Geoscience And Remote Sensing, 43*, 2148-2159.

Van Delm, A., & Gulinck, H. (2009). Classification and quantification of green in the expanding urban and semi-urban complex: Application of detailed field data and IKONOS-imagery. *Ecological Indicators, doi:10.1016/j.ecolind.2009.06.004.*